Soil Dynamics and Earthquake Engineering 173 (2023) 108056

Contents lists available at ScienceDirect

Soil Dynamics and Earthquake Engineering

journal homepage: www.elsevier.com/locate/soildyn

Earthquake-induced large deformations and failure mechanisms of silty sands in sloped ground conditions

Giuseppe Tomasello, Daniela Dominica Porcino *

Mediterranea University of Reggio Calabria – Dept. DICEAM, Via Zehender (Feo di Vito), 89122, Reggio Calabria, Italy

ARTICLE INFO

Keywords:
Non-plastic silty sand
Initial static shear stress
Cyclic simple shear
Failure mechanism
Undrained cyclic resistance
Pore-water pressure generation

ABSTRACT

In practical engineering, sand deposits or fills usually contain fines and are subjected to cyclic shear stresses induced by earthquakes, traffic, or waves which are superimposed on the initial static shear stress in natural or artificial slopes or beneath existing structures. To explore the combined and complex effect of an initial static shear stress and fines content of non-plastic silty sands on their deformation characteristics, pore pressure generation, and liquefaction susceptibility, the results of a comprehensive experimental program of cyclic simple shear (SS) tests are presented. Test conditions cover different fines contents f_c (0-40%), initial void ratios e_0, and initial static shear stress ratios (factor α=*0-0.30*). The observed types of failure are divided into four cyclic patterns: flow liquefaction, limited flow liquefaction, cyclic mobility, and plastic strain accumulation, depending on the initial state of the specimens and cyclic loading characteristics. Moreover, the threshold fines content (f_{thre}), denoting the specific value of the fines content at which the behavioral properties of the mixture are reversed, is not affected by α level, and a practically unique value of around 24.5% is identified. The K_α values of sand-silt mixtures measured under cyclic simple shear loading would either increase or decrease with an increasing initial static shear level based on the initial global void ratio and fines content of mixtures; in particular, for a given initial global void ratio, the reduction of cyclic resistance due to the addition of non-plastic fines ($f_c < f_{thre}$) is much more pronounced as α increases. Finally, the larger the initial shear stress, the smaller the cyclic pore-water pressure (*PWP*) measured at failure. Therefore, a modified stress-based *PWP* generation model is proposed to predict the cyclic residual excess pore pressures developed under various initial static shear stress conditions in non-plastic silty sands in a satisfactory way.

1. Introduction

For a soil element under sloping ground conditions (such as those found in dams and levees as well as near buildings) there exists initial static shear stresses on the horizontal plane, which can significantly affect the failure mechanisms, pore water pressure generation and liquefaction resistance of the soil. Case histories of liquefaction-induced failure in sandy soils in gentle slopes during recent earthquakes were reported by Kokusho [1] (Hokkaido-earthquakes in Japan) and by Porcino and Diano [2] and Chiaro and Koseki [3] (2012 Emilia Romagna earthquake in Italy).

The magnitude of the initial static shear stress level can be represented [4] by a normalized parameter, namely, the initial static shear stress ratio (α), which is defined as follows:

$$\alpha = \frac{\tau_{stat}}{\sigma'_{v0}} \tag{1}$$

where τ_{stat} is the static shear stress on the horizontal plane of a soil element, and σ'_{v0} is the effective vertical stress on the soil element.

Under cyclic loading conditions, the cyclic shear stress τ_{cyc} is superimposed with τ_{stat} and applied on the soil element so that shear stress reversal condition ($\tau_{cyc} > \tau_{stat}$) or no shear stress-reversal condition ($\tau_{cyc} \leq \tau_{stat}$) can occur with different resulting failure modes. In particular, the "cyclic mobility" pattern dominates for sand under the "stress reversal" conditions, and it is accompanied by a "butterfly" effective stress path and an S-shaped hysteresis loop [5]; the "plastic strain accumulation" is observed in the case of "no reversal" or "intermediate" stress conditions, characterised by the excessive development of residual strains on the side of the initial static shear [6,7]. Moreover, the flow liquefaction only occurs in loose sands, irrespective of the presence or

* Corresponding author.
E-mail addresses: giuseppe.tomasello@unirc.it (G. Tomasello), daniela.porcino@unirc.it (D.D. Porcino).

https://doi.org/10.1016/j.soildyn.2023.108056
Received 3 February 2023; Received in revised form 8 May 2023; Accepted 25 May 2023

absence of the initial static shear stress [8].

Most of the early investigations that considered static shear stress (or a preloading history) were triaxial tests on clean sands, where a specimen needs to be anisotropically consolidated to induce an initial static shear stress on the maximum shear stress plane [9–11]. Such studies demonstrated that factors such as density packing [6,12–14] and effective overburden stress [12,13,15], in addition to the material itself [12,16], are the key factors affecting the undrained cyclic strength of clean sands with the presence of an initial static shear stress.

Recognising that sandy soils containing silty fines may behave differently from those comprising pure clean sand, the effect of fines on the liquefaction susceptibility of soil mixtures has been extensively investigated through field and laboratory tests [17–21].

The undrained cyclic resistance was found to either increase or decrease with increasing f_c, depending on the state variable chosen for comparison, such as void ratio (e) [22,23], relative density (D_R) [24,25], and skeleton void ratio (e_s) [22,24]. Some researchers also used the equivalent intergranular void ratio (e^*) to unify the cyclic resistance of sand-fines mixtures [26]. Among these state variables, relative density has been commonly adopted as a state variable to characterise the cyclic resistance of clean sands, while controversial conclusions may arise when relative density is applied to sand-fines mixtures. This is probably due to uncertainties associated with measuring the maximum and minimum void ratios for soils with a fines content higher than 15% [27]. Yang et al. [28] investigated the rationale behind several state variables, including e, e_s and e^*, suggesting that the conventional void ratio remains a proper density index particularly suited to the framework of critical state soil mechanics. When compared at the same void ratio, the cyclic resistance of silty sands firstly decreases with increasing fines content up to a threshold fines content (f_{thre}), and afterward, it increases with fines content when $f_c > f_{thre}$. Hence, in sand-silt mixtures, threshold fines content (f_{thre}), also referred to as limiting fines content [29,30] and transitional fines content [31] in the literature, is the specific value of the fines content at which the way the fines influences the behavioral properties of the mixture is reversed [32]. Two main methods have been adopted for the experimental determination of the threshold fines content; namely, one that is based on a change of critical state parameters with fines content, and the other is based on the variation of the undrained cyclic strength (*CRR*) of the soil with fines content [31,33,34].

Few studies have investigated the initial static shear effect on the undrained cyclic behavior of silty sands with different fines contents [1,7,35–37], and further research is still needed even to identify the most suitable control variable to be used for the analysis of test results.

Kokusho [1] demonstrated through undrained cyclic torsional simple shear tests that an increase in non-plastic fines tends to shift loose sands from being dilative to contractive, and the failure mode under initial shear stress tends to change correspondingly from non-flow cyclic failure to flow-type failure.

Wei and Yang [7] performed a systematic study on the cyclic behavior and liquefaction resistance of silty sands (f_c was between 0% and 20%) through undrained cyclic triaxial tests with the presence of initial static shear stress. The authors provided a unified and consistent framework for interpreting the effects of initial static shear stress and quantifying such effects for engineering practice through correlations between *CRR* and state parameter (Ψ) for different fines contents at a given α level. Additionally, it was found that the *CRR*-Ψ lines rotated clockwise with increasing α. Moreover, it was found that the concept of threshold α (α_{th}) proposed by Yang and Sze [13] to characterize the impact of α on the cyclic resistance (*CRR*) of clean sands is applicable to silty sands as well [7]. In particular, when $\alpha < \alpha_{th}$, *CRR* increases with increasing α, otherwise it decreases with increasing α. The threshold α is affected by the initial packing density, initial effective confining pressure, and fines content [7].

To characterise the effect of α on cyclic liquefaction resistance, an initial static shear stress correction factor, K_α, was introduced by Seed [4]. It is defined as follows:

$$K_\alpha = \frac{CRR_{\alpha \neq 0}}{CRR_{\alpha=0}} \tag{2}$$

where $CRR_{\alpha \neq 0}$ and $CRR_{\alpha=0}$ are cyclic resistance ratios under different α values at the same initial packing density and effective confining pressure values. Thus, the effect of α on *CRR* will be beneficial or detrimental depending on whether K_α is > 1 or <1, respectively.

The effects of initial void ratio, confining pressure, material properties, and soil fabric on the K_α - α relationships were widely investigated for clean sands based on cyclic triaxial [6,11,38] or simple shear tests [12,15,39,40], although a consensus about using such correlations has not been found in the literature [12]. On the other hand, limited studies have investigated the K_α - α relationships of silty sand with variable fines contents [7].

The buildup of pore-water pressure (*PWP*) during undrained cyclic loading is the primary cause triggering excessive lateral deformations on the level ground or residual deformation accumulation on sloping ground, leading to catastrophic consequences in terms of damage [41]. Hence the assessment of *PWP* generation has received considerable attention [42–45]. The most relevant aspects being emphasized are: (i) the relationship between the residual pore-water pressure ratio and the normalized number of loading cycles is greatly influenced by the static shear stress [6,46,47]; (ii) at present, cyclic pore-water pressure models of silty sand rarely consider the influence of initial shear stress [36,46–48]. Consequently, studying the development mode of pore-water pressure of saturated silty sand under initial shear stress and establishing modified/new models is necessary.

This study focuses on the combined effect of initial static shear stress, and fines content on: a) failure mechanisms, b) cyclic liquefaction strength, and c) pore water pressure (*PWP*) generation of saturated silty sands during undrained cyclic loading. Constant volume simple shear (*SS*) test results from a comprehensive experimental program covering a wide range of global void ratio, non-plastic fines content (f_c = 0% - 40%), initial static shear stress ratio (α) value up to 0.30, and different applied cyclic stress ratios are presented. The cyclic SS device is considered to effectively mimic the anticipated stress conditions the soil would undergo during seismic loading. Finally, the effects of an initial static shear stress on the *PWPs* developed under cyclic loading of sands containing fines are investigated, considering both stress and strain-based *PWP* generation models. A new model is proposed to predict the increase in *PWP* during earthquakes in the natural or artificial slopes, dams, and embankments.

The experimental observations and quantitative findings obtained in the present study on the effect of an initial static shear stress on the undrained cyclic behavior of sands containing non-plastic or low plasticity fines can provide advancement for the practical design of engineering projects.

2. Materials and test procedure

The materials used for preparing specimens of sand-fines mixtures are clean sand and non-plastic silt. The host sand was Ticino sand (*TS*), a clean uniform size silica sand with a mean grain size (D_{50}) equal to 0.56 mm. The specific gravity G_S was 2.68, and the minimum and maximum void ratios according to ASTM D4253 [49] and ASTM D4254 [50] resulted in 0.58 and 0.93, respectively. The fines (d_{50} = 0.0245 mm) added to the host sand was a natural non-plastic silt collected from Ticino riverbank deposits. Six different fines contents ranging from 0% to 40% were used in the experimental investigation, namely 0%, 5%, 10%, 20%, 30%, and 40%, and the corresponding mixtures were labeled as *TS*, *TS5*, *TS10*, *TS20*, *TS30*, and *TS40*.

Fig. 1 illustrates the grain size distribution of the tested soils. For the tested mixtures of silt and sand, the particle diameter ratio χ introduced in the context of the binary packing theory [51] was calculated as the ratio between the diameter of sand particles at 10% passing (D_{10}) and

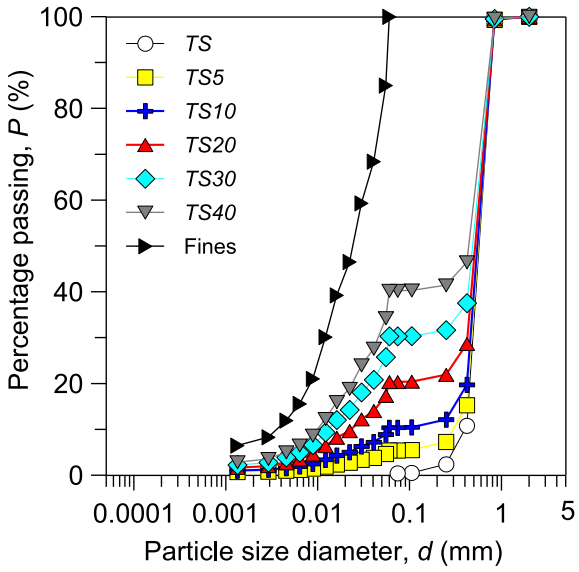

Fig. 1. Grading curves of tested materials.

the diameter of fines particles at 50% passing (d_{50}) [52]. The resulting particle diameter ratio χ of *TS*-fines mixtures was equal to 17.

The testing program comprised 140 constant-volume cyclic simple shear (CSS) tests performed at (i) different values of initial (post-consolidation) void ratio (e_0) ranging from 0.49 to 0.78, (ii) different values of initial static shear stress ratio (α) ranging from 0 to 0.30, and (iii) an initial effective vertical stress (σ'_{v0}) equal to 100 kPa. The testing program is given in Table 1.

Cyclic simple shear tests were performed using a modified NGI-type direct simple shear device [53]. The diameter and height of the specimens were 80 mm and 20 mm, respectively. In the NGI-type apparatus, lateral strains are prevented using a steel-wire reinforced rubber membrane. A constant-volume condition was achieved during shearing by keeping the sample height constant. The condition of constant sample height was performed by applying a decrease (or increase) of vertical stress ($\Delta\sigma_v$) through a closed loop control system, using feedback from the vertical displacement transducer to maintain the sample at the desired height actively. It is well known that $\Delta\sigma_v$ applied in a constant-volume SS test is essentially equal to the increase (or decrease) of excess pore water pressure (Δu) in a truly undrained SS test where the constant-volume condition is performed by a closed drainage system [54,55]. The validity of the constant volume approach has been verified by comparing the results of truly undrained and constant volume direct simple shear tests conducted on normally consolidated clays [55] as well as on sands [54,56–58].

In the present study the specimens were prepared to the desired void ratio by moist tamping in two layers without applying undercompaction [59]. First, dry sand and fines were mixed at the selected weight ratio, and an amount of de-aired water was added to the mixture, corresponding to a water content $w = 12.5 \pm 2.5\%$ for all tested fines contents; then, the reinforced membrane was filled with mixture, and each of the two layers was compacted to a given height. The values of w corresponded to a prefixed degree of saturation $S_r = 50\%$. Fifty percent saturation was chosen because it allowed for the preparation of specimens over a greater range of void ratios [30]. It was verified that the chosen water content ensures that the results are only marginally affected by suction [60]. In particular, the additional effective stress caused by soil suction, based on measurements performed by the Decagon WP4-T hygrometer, did not exceed ≅ 7 kPa even in specimens prepared with the highest fines content.

During the staged consolidation, several load increments were applied up to the target value of a vertical stress equal to $\sigma'_{v0} = 100$ kPa.

Table 1
Undrained cyclic simple shear tests ($\sigma'_{v0} = 100$ kPa).

Material	f_c (%)	e_0	α	CSR	$CRR_{N=15}$	$R_{u,res,f}$
TS	0	0.78	0	0.12-0.20	0.148	0.80-0.95
TS	0	0.78	0.10	0.08-0.14	0.124	0.68-0.88
TS	0	0.78	0.20	0.10-0.12	0.113	0.56-0.58
TS	0	0.78	0.30	0.10-0.12	0.103	0.41-0.42
TS	0	0.74	0	0.12-0.18	0.157	0.88-0.99
TS	0	0.68	0	0.14-0.23	0.177	0.77-0.93
TS	0	0.68	0.10	0.16-0.22	0.174	0.83-0.84
TS	0	0.68	0.20	0.16-0.20	0.167	0.64-0.75
TS	0	0.68	0.30	0.16-0.18	0.158	0.46
TS	0	0.63	0	0.20-0.25	0.208	0.92-0.95
TS	0	0.60	0	0.23-0.26	0.226	0.91-0.92
TS	0	0.60	0.10	0.23-0.28	0.231	0.82-0.88
TS	0	0.60	0.20	0.20-0.28	0.245	0.65-0.68
TS	0	0.60	0.30	0.22-0.28	0.259	0.41-0.43
TS5	5	0.73	0	0.10-0.16	0.131	0.86-0.99
TS5	5	0.68	0	0.14-0.16	0.153	0.88-0.97
TS5	5	0.61	0	0.14-0.22	0.172	0.93-0.99
TS10	10	0.68	0	0.14-0.16	0.129	0.94-0.97
TS10	10	0.68	0.05	0.14-0.16	0.136	0.95-0.98
TS10	10	0.68	0.10	0.08-0.12	0.108	0.79-0.82
TS10	10	0.68	0.20	0.08-0.10	0.088	0.60-0.62
TS10	10	0.68	0.30	0.03-0.06	0.052	0.43-0.45
TS10	10	0.60	0	0.14-0.20	0.161	0.93-0.98
TS10	10	0.60	0.05	0.16	–	0.92
TS10	10	0.60	0.10	0.14-0.19	0.157	0.84-0.90
TS10	10	0.60	0.20	0.12-0.16	0.141	0.59-0.69
TS10	10	0.60	0.30	0.08-0.12	0.094	0.36-0.45
TS10	10	0.55	0	0.14-0.20	0.181	0.94-0.98
TS10	10	0.55	0.10	0.17-0.22	0.182	0.90-0.93
TS10	10	0.55	0.20	0.18-0.23	0.191	0.74-0.75
TS10	10	0.55	0.30	0.16-0.18	0.191	0.55-0.57
TS10	10	0.53	0	0.16-0.19	0.202	0.95-0.96
TS20	20	0.68	0	0.08-0.12	0.106	0.95-0.98
TS20	20	0.68	0.10	0.04-0.10	0.059	0.66-0.85
TS20	20	0.59	0.10	0.10-0.12	0.108	0.81-0.94
TS20	20	0.59	0.20	0.08-0.10	0.090	0.60-0.66
TS20	20	0.58	0	0.12-0.16	0.127	0.95-0.98
TS20	20	0.55	0	0.14-0.20	0.146	0.95-0.98
TS20	20	0.55	0.10	0.14-0.20	0.147	0.92-0.93
TS20	20	0.55	0.20	0.13-0.16	0.144	0.67-0.74
TS20	20	0.55	0.30	0.14-0.16	0.144	0.51-0.58
TS20	20	0.51	0	0.14-0.19	0.168	0.97-0.99
TS30	30	0.68	0	0.08-0.14	0.102	0.87-0.95
TS30	30	0.68	0.10	0.06-0.10	0.067	0.85-0.90
TS30	30	0.59	0.10	0.10-0.12	0.116	0.89-0.95
TS30	30	0.59	0.20	0.08-0.10	0.089	0.45-0.66
TS30	30	0.58	0	0.12-0.18	0.125	0.93-0.98
TS30	30	0.55	0	0.16-0.20	0.183	0.93-0.96
TS30	30	0.55	0.10	0.16-0.19	0.177	0.90
TS30	30	0.55	0.20	0.14-0.16	0.147	0.71-0.72
TS30	30	0.55	0.30	0.12-0.14	0.130	0.49-0.52
TS30	30	0.49	0	0.20-0.24	0.214	0.86-0.93
TS40	40	0.68	0	0.10-0.16	0.138	0.86-0.92

After the end of the consolidation phase, when required, the specimens were subjected to static shear stress (τ_{stat}) on the horizontal plane under drained conditions to meet the desired value of shear stress ratio $\alpha = \tau_{stat}/\sigma'_{v0}$. The post-consolidation void ratio, e_0, which is identical to the void ratio prior to and during cyclic shearing, was used in the analysis of the tests reported in the following sections. Using the applied displacement sensors leads to an accuracy of about ±0.0015 in terms of void ratio. The measurements of vertical displacements were carried out with an LVDT (Linear Variable Differential Transducer, model W10TK, manufactured by H.B.M.) having a measuring range of 20 mm. The cyclic loading consisted of a symmetrical sinusoidal signal applied with a constant shear stress amplitude τ_{cyc}, corresponding to a certain cyclic stress ratio $CSR = \tau_{cyc}/\sigma'_{v0}$. It was applied in load-controlled mode at a frequency of 0.10 Hz which was chosen to ensure better control of undrained/constant volume test conditions [53]. A continuous record of all measured data was realized through a data acquisition system connected to a computer. The development of the shear stress (τ), vertical stress

(σ_v), and shear strain (γ) with time were recorded. All tests were conducted until a single amplitude shear strain (γ_{SA}) or a peak shear strain (γ_{peak}), in the order of 3.75%, was reached, and this strain-based criterion was selected for liquefaction or failure, respectively.

3. Typical cyclic failure patterns of silty sands with presence of τ_{stat}

Four main typical failure patterns, namely flow liquefaction, limited flow liquefaction, cyclic mobility, and plastic strain accumulation were observed in the cyclic simple shear tests performed in the present study.

Fig. 2a presents test results from a *TS20* specimen ($e_0 = 0.68$, $\sigma'_{v0} =$ 100 kPa) with an initial static shear stress ratio α equal to 0.10. The stress-strain (τ-γ) relationship shows that initially a limited increase in shear strains occurs, but suddenly a dramatic rise of γ takes place with an unstable response. After the occurrence of flow failure, the effective stress path moves to the critical state (Fig. 2a), indicating that a failure state has been reached. This type of failure, referred to as "cyclic flow liquefaction," was observed in the case of materials tested at higher void ratio (i.e. $e_0 \geq 0.68$) with fines content in the range from 20% to 30%.

Fig. 2b presents the test results of a *TS30* specimen exhibiting limited flow liquefaction ($e_0 = 0.68$, $\sigma'_{v0} = 100$ kPa, $\alpha = 0$). The shear strains initially do not accumulate significantly, whereas when the flow is triggered, very large shear strains immediately increase and essentially stop after cyclic loading.

The undrained cyclic response of a silty sand specimen exhibiting a cyclic mobility failure mechanism is presented in Fig. 3a. In this kind of behavior, the effective stress path gradually moves leftward with the number of applied cyclic loading to a transient quasi-zero effective stress state (Fig. 3a). When this state is attained, significant shear strain development occurs during the subsequent cycles. After the loading is reversed, the specimen regains its stiffness and strength due to the decrease in pore water pressure and the corresponding increase in the effective vertical stress. This failure occurred for specimens exhibiting a hardening behavior under stress reversal conditions.

Fig. 3b presents the results of an undrained cyclic SS test conducted on *TS20* tested with $\alpha = 0.20$ exhibiting plastic strain accumulation. Irrecoverable residual shear strains accumulated on the positive side with increasing loading cycles. The effective vertical stress gradually decreased and finally became stable in correspondence with the critical state line (Fig. 3b). This type of failure may occur when the specimens are loaded without stress reversal and satisfy the requirement of an initial state capable of inducing a hardening behavior. However, this kind of behavior was observed even with a limited shear stress reversal condition (i.e., α/CSR>0.71).

For all types of cyclic response (Figs. 2 and 3), the mobilised internal friction angle at the ultimate state of the CSS tests (when the specimen attains failure conditions) resulted in relatively good agreement with the

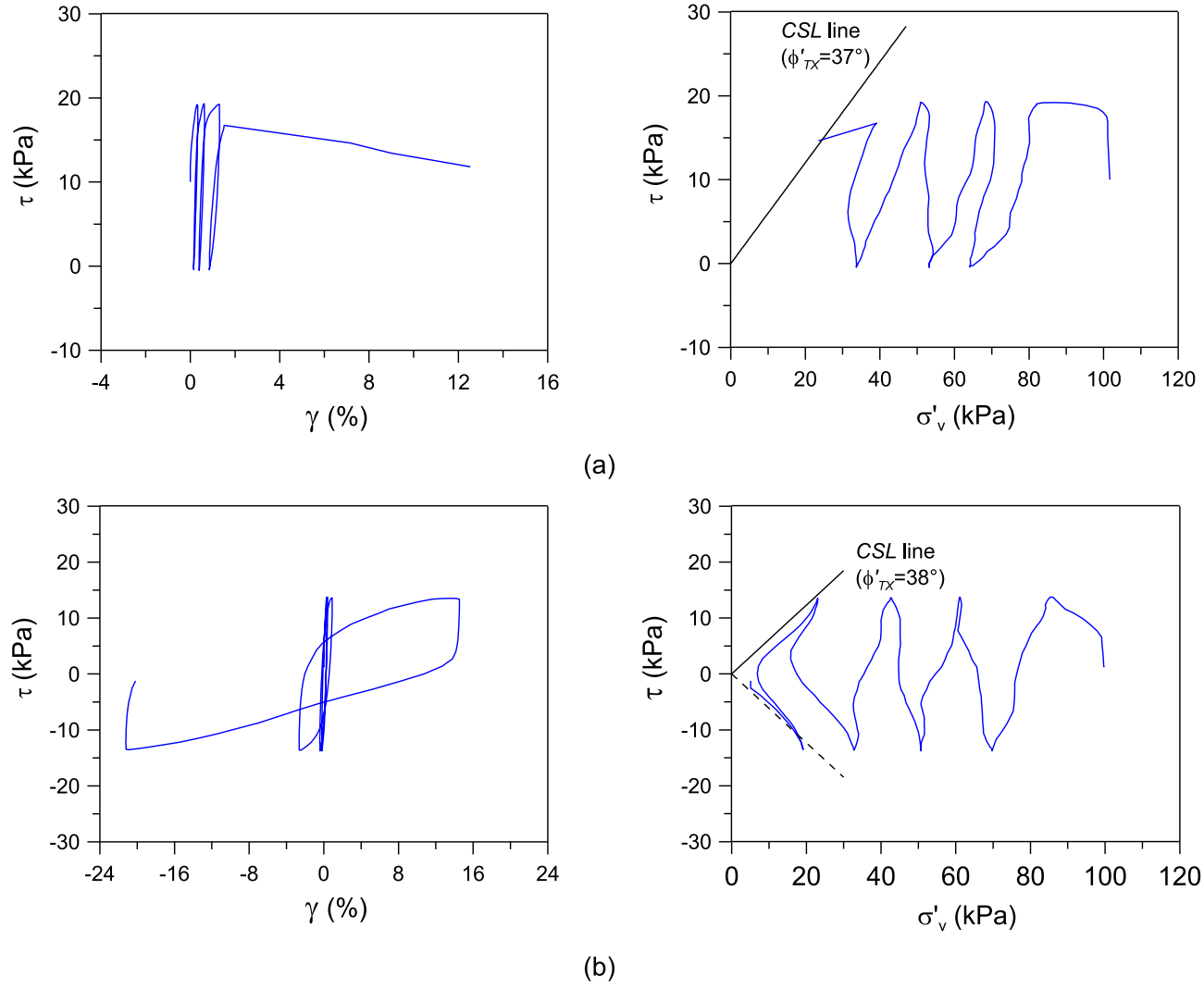

Fig. 2. Typical flow type failures of silty sands from cyclic simple shear tests: (a) flow liquefaction (TS with f_c=20%; e_0=0.68; α=0.10; σ'_{v0}=100 kPa); and (b) limited flow liquefaction (TS with f_c=30%; e_0=0.68; α=0; σ'_{v0}=100 kPa).

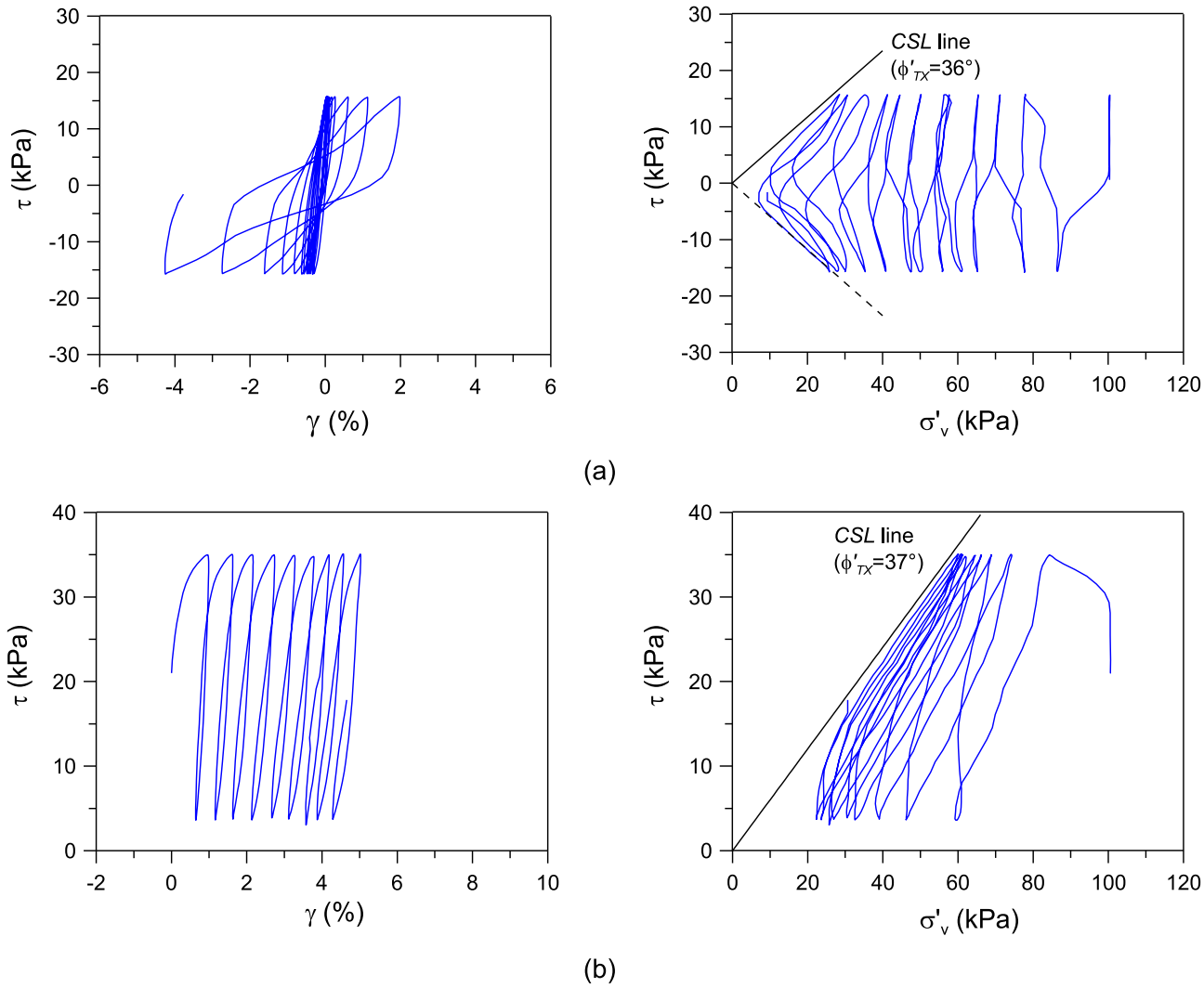

Fig. 3. Typical non-flow type failures of silty sands from cyclic simple shear tests: (a) cyclic mobility (TS with f_c=10%; e_0=0.60; α=0; σ'_{v0}=100 kPa); and (b) plastic strain accumulation (TS with f_c=20%; e_0=0.55; α=0.20; σ'_{v0}=100 kPa).

value of critical state internal friction angle determined for the same material from undrained monotonic triaxial compression tests [61].

As discussed previously, there are mainly four distinct failure patterns. Different failure patterns correspond to different features of strain development and excess pore water pressure generation. The failure criteria for cyclically loaded specimens are commonly defined

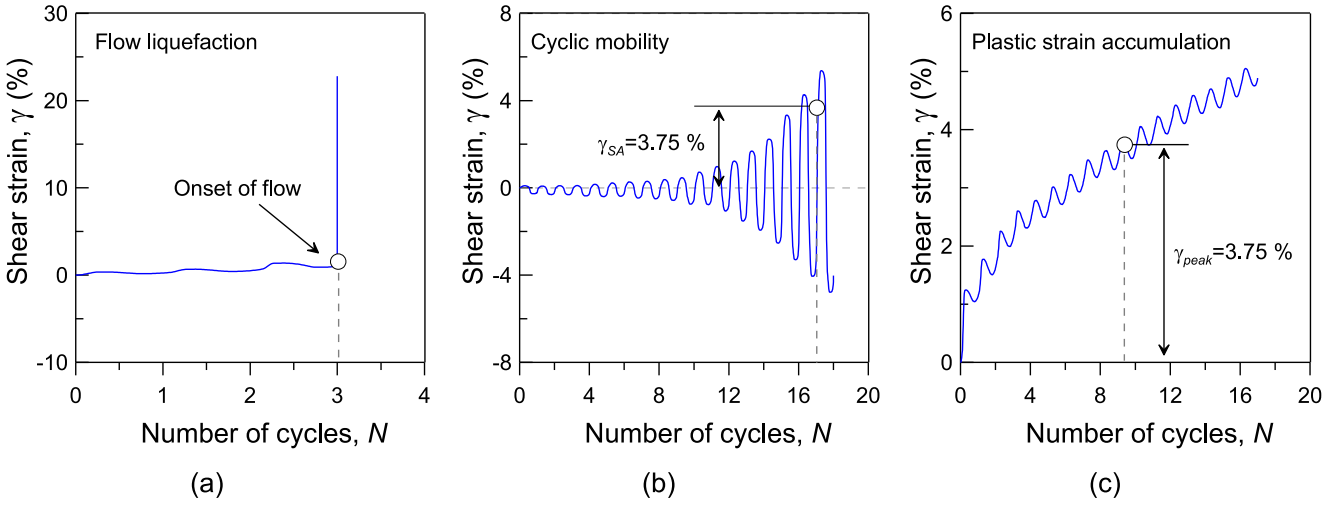

Fig. 4. Shear strain development for different cyclic failure patterns: (a) flow liquefaction, (b) cyclic mobility and (c) plastic strain accumulation.

through the development of excess pore water pressures or shear strains. In the present study, the criterion based on the development of shear strains turned out to have more general validity, irrespective of the failure pattern.

Fig. 4 presents the development of shear strains with the number of cycles observed in CSS tests exhibiting each failure pattern. It can be observed that:

a) In the case of flow failure, the point at which the shear strains start to increase sharply was assumed for the onset of liquefaction (Fig. 4a).
b) The shear strains in the tests exhibiting cyclic mobility change cyclically between the positive and negative sides (Fig. 4b). For this reason, a failure criterion based on a single amplitude shear strain equal to 3.75% was adopted [62].
c) Finally, in the case of plastic strain accumulation behavior, an accumulated peak shear strain equal to 3.75% was used to identify failure conditions (Fig. 4c).

4. Analysis of test results

4.1. Cyclic liquefaction resistance curves

The cyclic resistance ratio (*CRR*) is defined as the *CSR* causing failure at a given number of loading cycles. It is commonly determined using the relationship between *CSR* and the number of cycles that the soil can sustain until failure/liquefaction (N_f). Fig. 5 presents selected *CSR*-N_f relationships for Ticino sand-silt mixtures in the presence and absence of α. A power law equation was adopted to describe the *CSR*-N_f relationships over the range of *N* values relevant to earthquake loading:

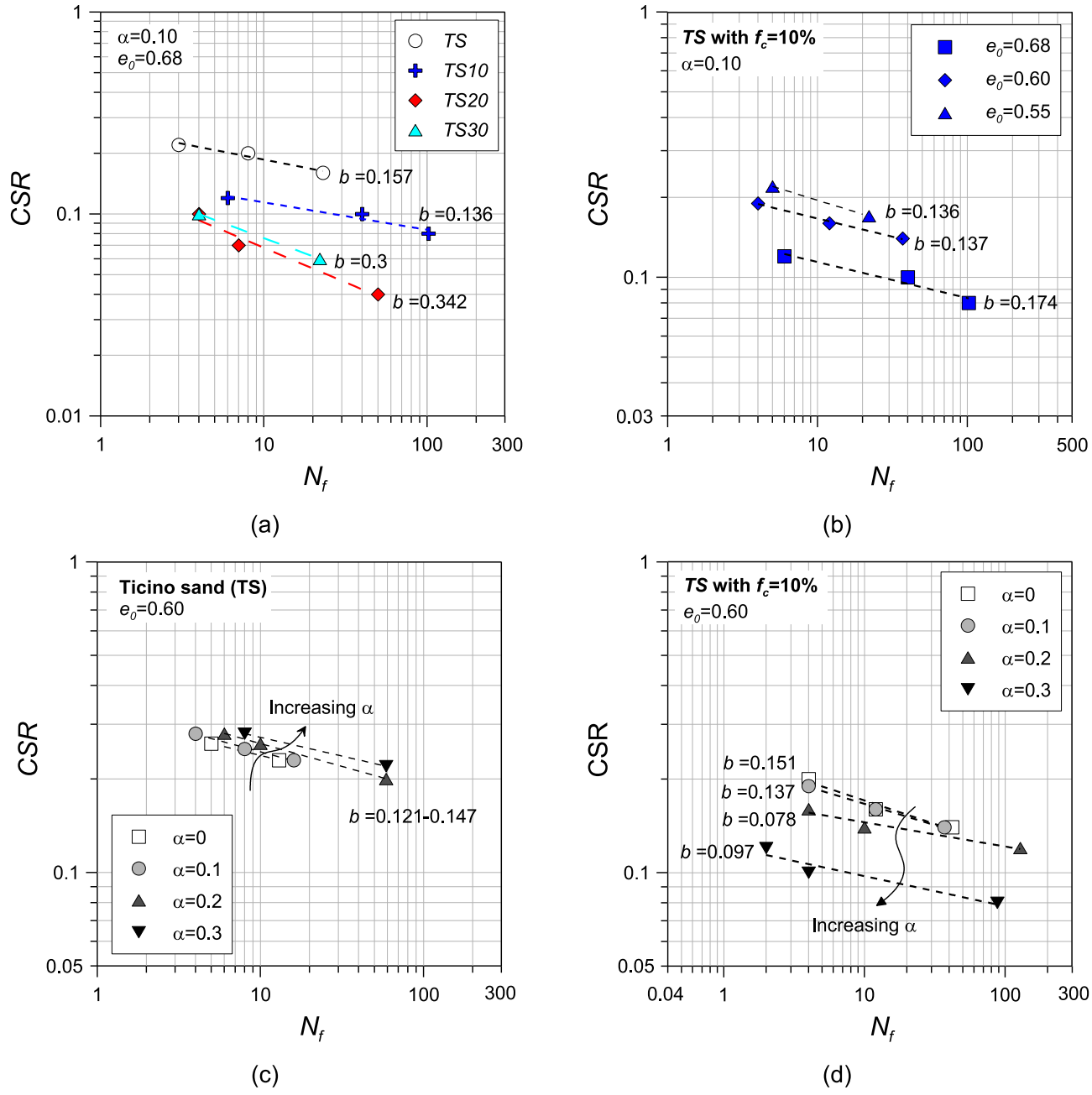

Fig. 5. Typical *CSR*–N_f relationships for Ticino sand silt mixtures (σ'_{v0}=100 kPa): (a) effect of f_c with $\alpha \neq 0$, (b) effect of e_0 with $\alpha \neq 0$, (c) and (d) effect of α.

$$CSR = a \bullet N_f^{-b} \quad (3)$$

where a and b are positive fitting parameters, in particular, b is the fitting parameter describing the slope of the straight line replotting the data on a log-log plot.

Fig. 5 displays the main factors affecting the cyclic liquefaction resistance of Ticino sand with non-plastic fines, i.e., fines content, (global) void ratio, and initial static shear stress. Fig. 5a suggests that if the initial global void ratio (e_0) is used as the basis for comparison, as the content of silt increases up to a threshold f_c value (in the range from 20% to 30%), the undrained cyclic strength of the mixture decreases. Beyond the threshold value of f_c, the tendency is reversed, namely increasing fines content raises soil resistance to liquefaction. Fig. 5a refers to CSS tests performed at $\alpha = 0.10$; as will be shown later, a suggested methodology has been proposed to accurately identify the value of f_{thre} for both $\alpha = 0$ and $\alpha \neq 0$ CSS tests.

Fig. 5a shows the values of fitting parameter b (Eq. 3) in the range 0.30-0.342 for higher fines content (f_c = 20%, 30%), whereas for lower fines content b values are in the range 0.136-0.157. *CSS* tests performed on sand-silt mixtures in the absence of α have also shown similar trends. An analogous trend of b values with fines content was observed also by other authors in undrained cyclic torsional shear tests on sand-fines mixtures in the absence of an initial static shear stress [63].

Another factor that may influence the cyclic liquefaction resistance of silty sands is the void ratio (e_0). Fig. 5b shows the curves of cyclic stress ratio versus the number of cycles to failure for specimens of *TS* with 10% fines content (α = 0.10) tested at different e_0 values (0.55–0.68). As shown in Fig. 5b, the cyclic resistance of silty sands decreases with increasing void ratio, and the *CSR*-N_f trend lines shift downwards with increasing e_0.

The impact of void ratio on b values (Fig. 5b) appears insignificant since they are between 0.136 and 0.174. Similarly, the analysis of both

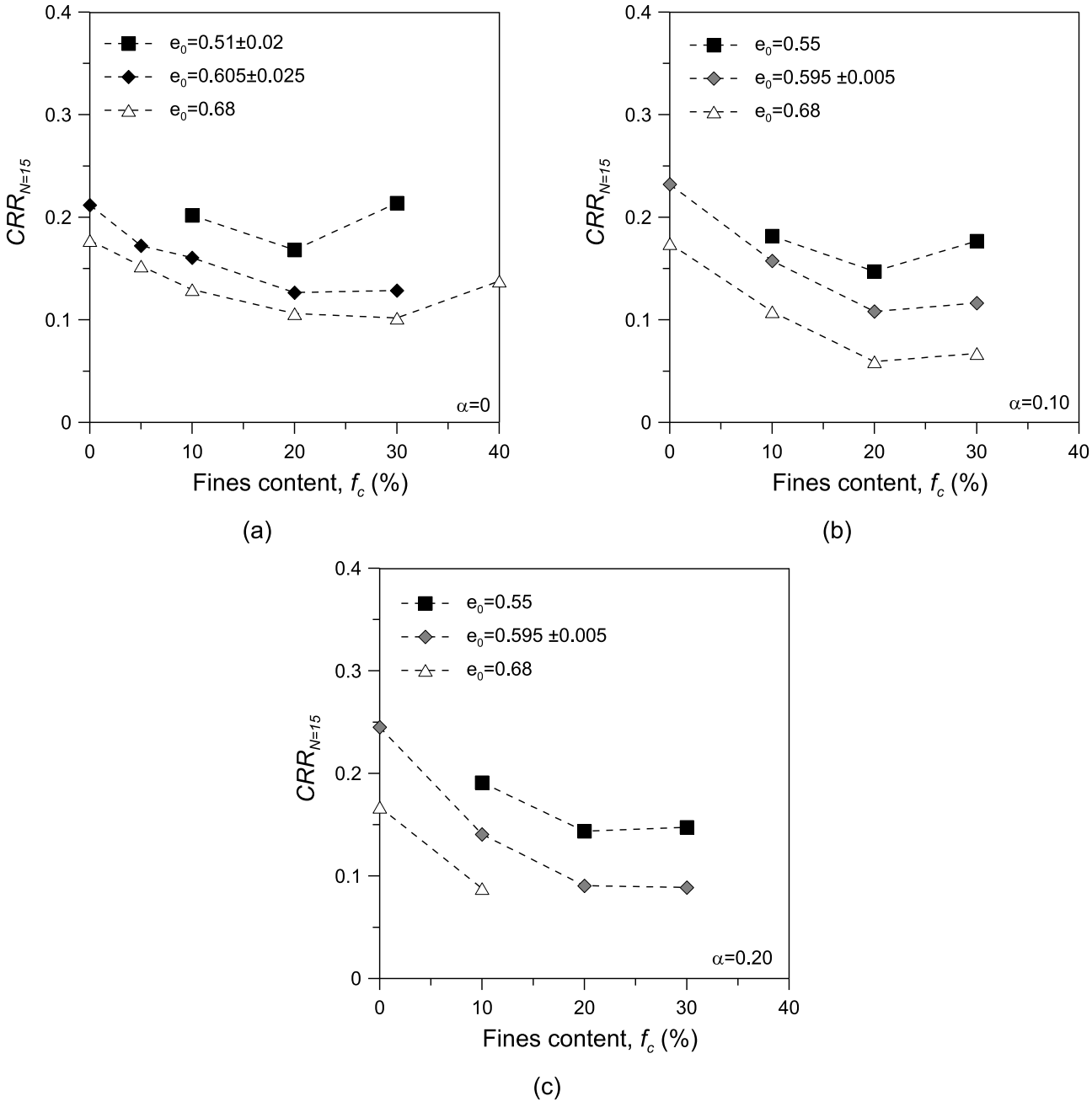

Fig. 6. Effect of fines content and void ratio on the undrained cyclic resistance of silty sands for: (a) α=0, (b) α=0.1 and (c) α=0.2 (σ'_{v0}=100 kPa).

symmetrical and non-symmetrical *CSS* tests performed on the Ticino clean sand mixed with 0%, 20%, and 30% fines content does not evidence an apparent trend with respect to e_0.

The effect of α on the cyclic strength of silty sands can be either beneficial or detrimental, mainly depending on fines content and initial void ratio. Fig. 5c and 5d show the effects of α on the *CSR*-N_f relationships for *TS* and *TS10*, respectively, tested at a relatively low void ratio (e.g., $e_0 = 0.60$). The effect of α is positive for Ticino sand, whereas, for *TS10*, the effect of α is negative, causing a decrease in the undrained cyclic strength of the material.

Fig. 5c also shows that the slope of the *CSR*-N_f lines is in a narrow range of 0.121-0.147 with respect to α values. Nevertheless, when the effect of α on *CRR* is detrimental (Fig. 5d), b values decrease apparently with increasing α level. This trend was observed in the present study not only for *TS10* but also for all tested mixtures (f_c = 0-30%).

To characterise the effect of α and f_c on cyclic liquefaction resistance of *TS*-silt mixtures, in the following, the results will be analysed in terms of the initial static shear stress correction factor, K_α, and the fines content correction factor, K_{fc}, respectively.

4.2. K_{fc} correction factor of CRR for fines content

Fig. 6 shows the variation of $CRR_{N=15}$, i.e. the cyclic stress ratio (*CSR*) causing liquefaction in 15 uniform loading cycles, in terms of fines content and e_0 for all mixtures studied under different initial static shear stress ratios. In engineering practice, the typical number of equivalent uniform cycles of an earthquake is related to the moment magnitude (M_w) of the earthquake (e.g. [64–66]). In liquefaction analyses, a reference earthquake of magnitude M_w = 7.5, corresponding to 15 uniform loading cycles, is usually adopted [67,68]; therefore, in the present study, N_f = 15 has been considered for the analysis of experimental results.

It can be observed from Fig. 6 that in both cases (α=0 and $\alpha\neq$0), *CRR* tends to decrease with the addition of fines content up to the threshold fines content ranging qualitatively between 20% and 30%. This trend is more pronounced for specimens subjected to initial static shear stresses ($\alpha\neq$0) compared to that observed in companion tests with α = 0. Conversely, a slight tendency of *CRR* to increase is observed for higher fines content in the tests with α = 0 compared to that observed in companion tests with $\alpha\neq$0. Additionally, it is interesting to note that the sensitivity of *CRR* to the void ratio is affected by α if the data were compared for the same material. In particular, the *CRR* decreases more significantly with a specific increment of void ratio for higher α values (i.e., α = 0.2) than for lower ones (i.e., α = 0). A similar observation was found by Wei and Yang [7] in cyclic triaxial tests on Toyoura sand mixed with non-plastic silt.

As suggested by Bouckovalas et al. [69] and Polito and Martin [70], the effect of fines on liquefaction resistance can be well described through a correction factor K_{fc}, defined by the following expression:

$$K_{fc} = \frac{CRR_{fc}}{CRR_{fc=0}} \tag{4}$$

where CRR_{fc} and $CRR_{fc=0}$ are respectively the cyclic resistance ratios corresponding to the same number of cycles evaluated for silty sand and clean sand, tested at the same (global) void ratio and the same initial effective vertical stress. When f_c = 0, K_{fc} = 1 from Eq. (4).

Fig. 7 presents the measured K_{fc} – f_c relationships of *TS*-fines mixtures at different initial void ratios (e_0 = 0.58–0.74) for all α levels. Consistency with the trend of the curves $CRR_{N=15}$ vs. f_c reported in Fig. 6, it can be observed (Fig. 7) that also K_{fc} tends to initially decrease with f_c, indicating that the effect of fines content is detrimental, and this reduction is more pronounced when the static stress ratio α becomes higher. This trend continues up to the threshold fines content f_{thre} after which the trend reverses. Although some scatter can be observed in some curves (Fig. 7), no significant dependence of K_{fc} on void ratio was found, consistent with the findings gathered from undrained cyclic triaxial tests on mixtures of sand and silt carried out by previous researchers [7,71].

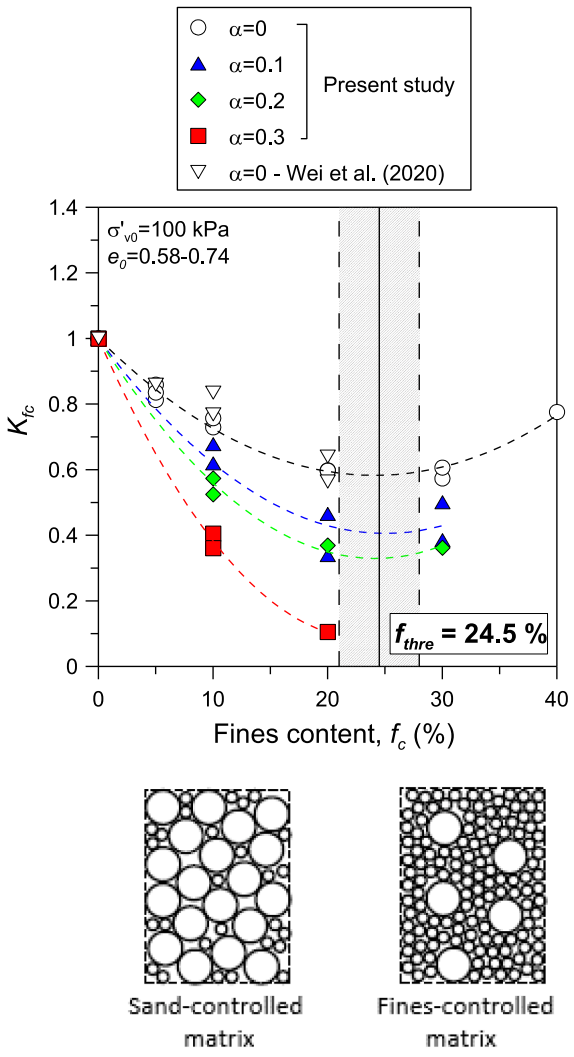

Fig. 7. Identification of f_{thre} by undrained cyclic simple shear tests performed on TS-silt mixtures with and without the presence of τ_{stat}.

To properly account for the variation of cyclic resistance of sand due to fines, a simple, explicit law can be usefully proposed. In general, a linear function has been proposed in the literature to depict clearly the trend of K_{fc} versus f_c [69,71]. However, it should be noted that a linear relationship is inadequate for the Ticino sand-silt mixtures studied in the present research because the K_{fc} - f_c relationship is markedly non-linear (Fig. 7). This holds true for all initial static shear stresses considered in the present study (α = 0–0.30).

In the present study, a parabolic law is proposed to characterise the trend of the K_{fc} - f_c relationship exhibited by the Ticino sand-silt mixtures (R^2>0.96) (Fig. 7), namely:

$$K_{fc} = 1 - g \bullet f_c + h \bullet (f_c)^2 \tag{5}$$

where g and h are empirical coefficients depending on the magnitude of the initial static shear stress ratio applied, and f_c is expressed in percentage. Nevertheless, it cannot be excluded that, generally, g and h are also influenced by other factors such as mean effective stress, grading characteristics, grain shape, etc.

Notwithstanding this circumstance, for the silty sands considered in the present research (f_c = 0–40%; σ'_{v0} = 100 kPa; α = 0–0.30; χ = 17), the following linear relationships were found appropriate:

$$g = 0.0331 + 0.1397 \bullet \alpha \quad (6)$$

$$h = 0.0006 + 0.0032 \bullet \alpha$$

The two equations reported above are characterised by a coefficient of determination R^2 equal to 0.95.

The values of K_{fc} predicted by Eqs. (5) and (6) were found to be consistent with those obtained experimentally by Wei et al. [71] on Toyoura sand-fines mixtures from undrained cyclic triaxial tests (Fig. 7).

A practically unique average value of threshold fines content around 24.5% was identified from Fig. 7 for all α levels. It was determined considering the minimum of Eq. (5) for each α level identifying a narrow-bounded zone, as sketched in Fig. 7.

Conceptually, when the fines content is less than f_{thre}, the microstructure of the granular mix is defined (and the deformational behavior is controlled) by the sand matrix. On the other hand, at fines content higher than f_{thre}, the microstructure is controlled by the fine matrix, i.e. by the smaller grains (silt particles). Indeed the concept of a threshold fines content, f_{thre}, which demarcates a fines-in-sand from a sand-in-fines matrix, is an idealisation of a transition zone that can be more or less wide.

Several authors have proposed alternative calculation methods in the literature [29,30,72], which were based on the simple knowledge of some physical and grading features of sand-silt mixtures. The average experimental value of f_{thre} in the present study was found to be in reasonably good agreement with $f_{thre} = 23\%$ resulting from Hazirbaba's equation [29].

Finally, K_{fc} can serve as a standardised basis to compare the data from different studies and, at the same time, accurately identify the threshold fines content of sand-silt mixtures, even with the presence of an initial static shear stress.

4.3. K_α correction factor of CRR for initial static shear stress

To quantify the effect of α, an initial static shear stress correction factor, K_α, was introduced by Seed [4] through Eq. (2).

The impact of initial global void ratio and fines content on K_α - α correlations are presented in Figs. 8 and 9, respectively. The K_α - α curves for clean sand are drawn in Fig. 8a. Fig. 8a shows that the specimens in a

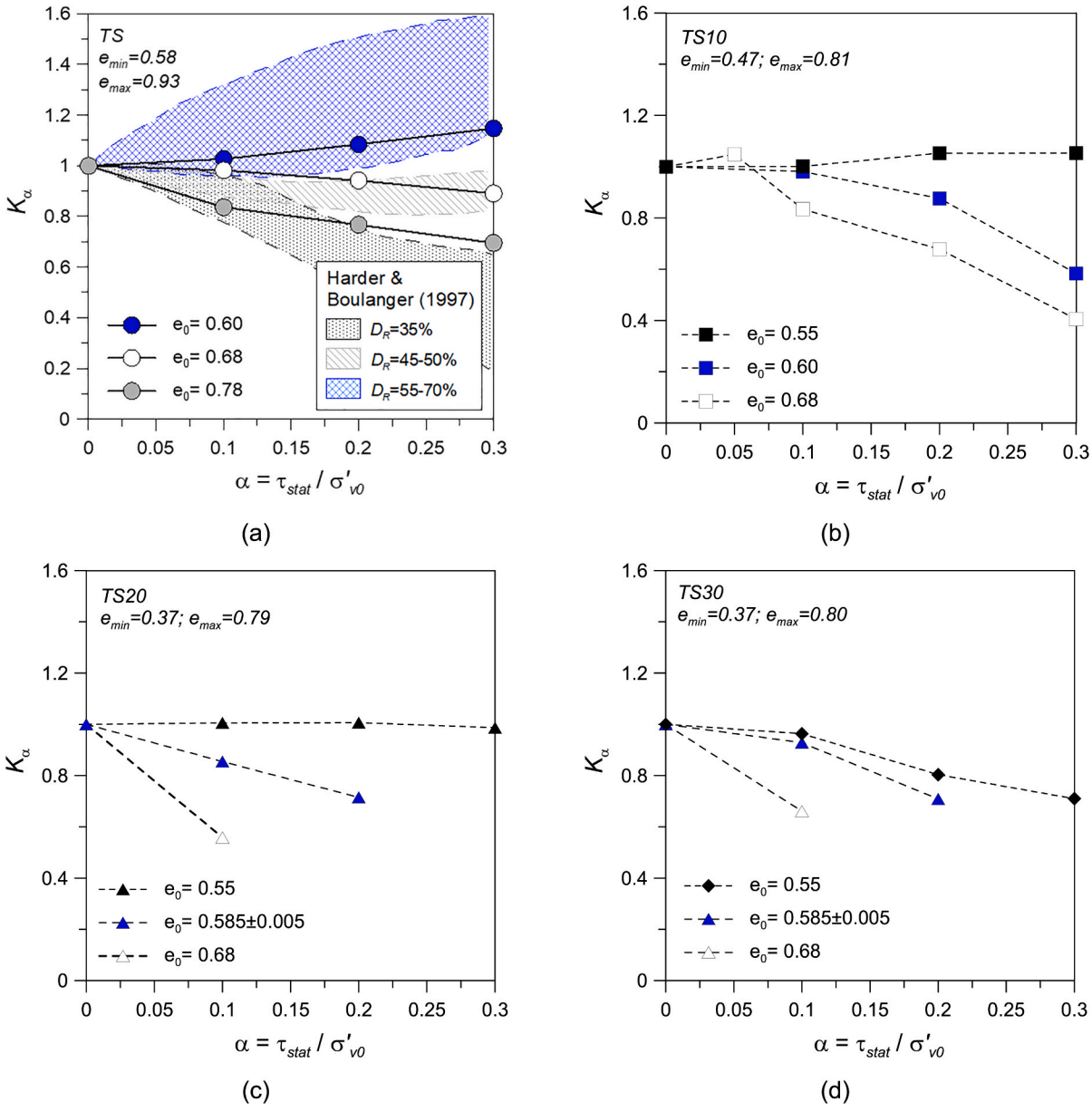

Fig. 8. K_α-α correlations for Ticino silty sand considering the effect of void ratio (σ'_{v0}=100 kPa): (a) *TS*; (b) *TS10*, (c) TS20 and (d) *TS30*.

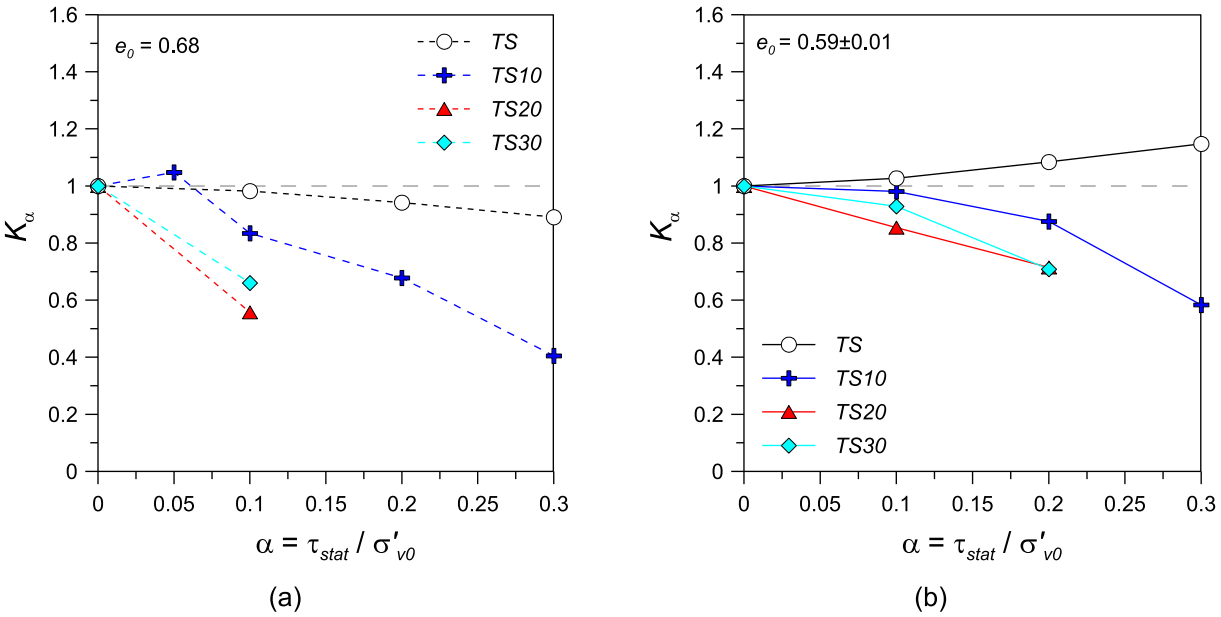

Fig. 9. Effects of fines content on K_α correction factor of *CRR* for initial static shear stress (σ'_{v0}=100 kPa).

dense state ($e_0 = 0.60$, $D_R = 94\%$) exhibit an increase in the undrained cyclic resistance as α increases, whereas specimens in a medium-dense state ($e_0 = 0.68$, $D_R = 71\%$) and in a loose state ($e_0 = 0.78$, $D_R = 43\%$) show a reduction in the undrained cyclic resistance ($K_\alpha < 1$) as α increases. The results obtained in the present study were also compared with the correlations proposed by Harder and Boulanger [73] for clean sands. The results show that Harder and Boulanger [73] yield higher K_α values than those obtained in the present study for *TS*, especially for medium-dense/dense sands (Fig. 8a) [74].

Literature review clearly shows that, in addition to the relative density, the K_α-α relationships of clean sands are affected by many other factors such as particle gradation and shape [12], mineralogical features of sand [75], sample preparation methods [38], initial effective vertical stress [12,15,40], failure criterion [14], and test apparatus [12,15]. This justifies to some extent the large bounding regions proposed by Harder and Boulanger and the controversial results obtained in different research.

Of particular concern are the results obtained for Ticino silty sand mixtures with a percentage of fines equal to 10%, as shown in Fig. 8b. In this case, an initial static shear stress can entail a limited increase ($K_\alpha > 1$) or a significant reduction in the cyclic undrained resistance ($K_\alpha < 1$) as α increases, depending on the value of the initial global void ratio of the material. In particular, passing from a relatively low void ratio ($e_0 = 0.55$) to a relatively high void ratio ($e_0 = 0.68$), a significant loss of the undrained cyclic resistance is observed with increasing α.

The results for silty sand with f_c equal to 20% and 30% at the same initial global void ratio $e_0 = 0.55$ show that the cyclic undrained resistance of the material does not significantly vary ($K_\alpha \approx 1$) ($f_c = 20\%$) or slightly vary ($f_c = 30\%$) with the parameter α. For the other analysed initial global void ratios, a reduction of K_α is observed for both mixtures (*TS20* and *TS30*).

For the materials and initial test conditions studied in the present research, the existence of a threshold α value [13] was not found except for *TS10* prepared at $e_0 = 0.68$, where the effect of α resulted initially positive and afterward negative beyond a specific value of α ($\alpha_{th} \cong 0.05$). This aspect would require a thorough consideration of all factors affecting α_{th}, such as void ratio, initial mean effective stress, fines content, grading features of the base sand and the fines, etc.

The impact of fines content on K_α - α correlations is presented in Fig. 9. As discussed in Fig. 7, the reduction of cyclic resistance due to the addition of non-plastic fines ($f_c < f_{thre}$) was much more pronounced as α increased, i.e., passing from a level ground (α=0) to sloping ground ($\alpha \neq 0$) conditions. Additionally, Fig. 9 shows that when the results are compared at the same global void ratio, the cyclic resistance reduction due to an initial static shear stress is much more pronounced as fines content increases up to the threshold fines content.

Thus, for the silty sands tested in the present study, e_0 and fines content play an essential role in the K_α-α relationships.

4.4. MSF magnitude scaling factor

Values of the normalized cyclic stress ratio ($CSR_N/CSR_{N=15}$) against the number of cycles to liquefaction are plotted in Fig. 10a for all *TS*-fines mixtures. Although some scatter can be observed, interestingly, Fig. 10a displays that a practically single trendline can be drawn for the entire data set of mixtures tested in the current study (for a total number of tests equal to 134), regardless of initial global void ratio, fines content, and initial static shear stress ratio.

Other researchers (e.g. [27]) obtained a unique relationship between the normalized cyclic stress ratio and the number of cycles to liquefaction based on cyclic triaxial tests performed on two sands mixed with non-plastic silica silt, regardless of void ratio, confining pressure, fines content and base sand type as well.

Cyclic liquefaction resistance curves obtained from the laboratory can be used to derive magnitude scaling factors *MSFs* for soil liquefaction evaluation under earthquakes of different magnitudes M_w.

MSF is defined as:

$$MSF = \frac{CSR_M}{CSR_{M=7.5}} \tag{8}$$

Thus, the relationship shown in Fig. 10a may be further developed into the relationship between the magnitude scaling factor (*MSF*) and the moment magnitude (M_w) of an earthquake, as shown in Fig. 10b. It was achieved by relating N_f to M_w according to the suggestion of Idriss [65]. The *MSF* relationship plotted in Fig. 10b is expressed as:

$$MSF = 2.536 \bullet exp\left(-\frac{M_w}{8.083}\right) \tag{9}$$

providing a coefficient of determination R^2 equal to 0.83.

The *MSF* relationship derived by the present study was compared with other *MSF*-M_w correlations proposed in the literature. The series of

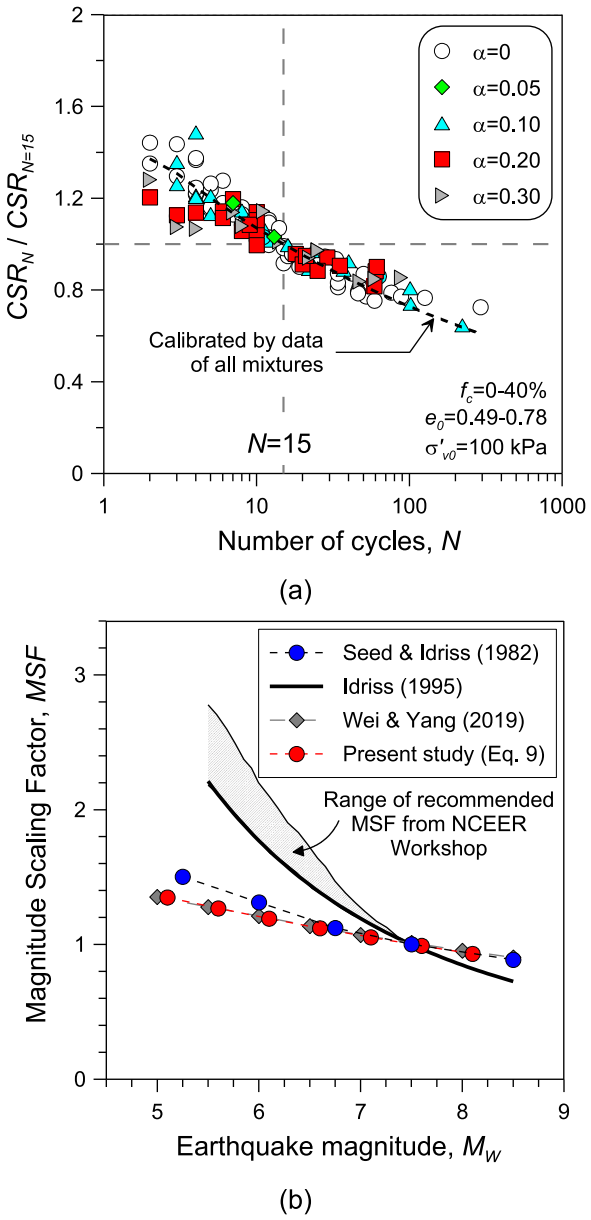

Fig. 10. Unified relationship between N_f and normalized cyclic stress ratio for Ticino-fines mixtures over a wide range of void ratio and α levels (a) and MSF derived by several investigators (b).

magnitude scaling factors derived from Ticino sand-silt mixtures coincide with those suggested by Wei and Yang [27], noting that their proposal was also based on laboratory investigation into reconstituted sand mixed with non-plastic silt (α=0). Additionally, the magnitude scaling factors calibrated from Ticino sand-silt mixtures data (α=0 and $\alpha\neq$0) are only slightly lower than the original *MSF* suggested by Seed and Idriss [64], which were calibrated by laboratory tests on clean sands (α=0). It would suggest that the relation proposed by Seed and Idriss [64] applies to non-plastic silty sands regardless of fines content, void ratio, and static shear stress level. Youd et al. [67] recommended that the shaded area, i.e. the range of recommended *MSF* from the NCEER Workshop, be used for engineering practice when $M_w < 7.5$, while they recommended the values suggested by Idriss (1995) to be applied for $M_w > 7.5$. These *MSF* values are significantly higher than those derived in the present study from simple shear tests using a variety of sand-non-plastic fines mixtures, void ratios, and static shear stress conditions, showing poor consistency.

Additional studies are needed to further improve the *MSF* relationships in liquefaction triggering analyses to turn the CRR_{10} or CRR_{15} to a cyclic resistance ratio under a certain magnitude of an earthquake, based on the examination of cyclic testing results for a broad range of non-plastic silty sands and initial stress conditions.

4.5. Pore water pressure generation and modelling

Different approaches were proposed in the literature to predict the cyclic excess pore water pressure generation in saturated sandy soils, which are grouped under the headings of (i) stress-based models (e.g. [44,76,77]), (ii) strain-based models (e.g. [78,79]), (iii) energy-based models (e.g. [45,80,81]), and (iv) plasticity theory-based models (e.g. [82,83]). In the present study, stress-based and strain-based *PWP* models were used for interpreting the experimental results of undrained *CSS* tests with varying initial static shear stresses and fines contents.

During stress-controlled cyclic tests, the residual pore water pressures (Δu_{res}) are those presented at the time when the applied shear stress was equal to or crossed zero. The residual excess pore pressure ratio ($R_{u,res}$) is defined as the ratio of the residual excess pore pressure to the initial effective vertical stress (σ'_{v0}) acting on the soil ($R_{u,res} = \Delta u_{res}/\sigma'_{v0}$).

Fig. 11 shows $R_{u,res}$ against the number of cycles N, normalized by the number of cycles required for attaining liquefaction (N_f) for *CSS* tests under symmetrical (α=0) and non-symmetrical ($\alpha\neq$0) stress conditions. The data points refer to various amplitudes of cyclic stresses *CSR* (0.03–0.28), percentages of fines f_c (0-30%), and post-consolidation void ratio e_0 (0.49–0.78). As shown in Fig. 11a, the $R_{u,res}$ increases quickly in the early cycles. Subsequently, its rate becomes moderate before sharply increasing to the limiting value, ranging from 0.77 to 0.99. It is interesting to note that when γ_{SA} attains 3.75% (N=N_f), the $R_{u,res}$ values did not reach 100%. This experimental evidence is consistent with that reported by previous research conducted on clean sands and silty sands [2,24,84,85]. This initial upward convex trend followed by an upward concave trend of the *PWP* generation curve is generally a characteristic of silty sands with a percentage of fines up to the f_{thre}. Nevertheless, Fig. 11a highlights that this trend holds true also for *TS30*. A possible explanation for this may be attributed to the fact that $f_c = 30\%$ is only slightly higher than the threshold fines transition zone (Fig. 7).

Seed et al. [76] proposed an empirical model to predict the pore water pressure generation of sand based on extensive stress-controlled undrained cyclic simple shear tests. The model was subsequently simplified by Booker et al. [86] as in the following:

$$R_{u,res} = \frac{2}{\pi} \bullet arcsin\left[\frac{N}{N_f}^{\left(\frac{1}{2\bullet\beta}\right)}\right] \quad (10)$$

where the fitting parameter β ranges from 0.6 to 1, a value of β equal to 0.7 is generally assumed and recommended by Seed et al. [76] for clean sands.

The upper and lower bounds of the experimental data points for the Ticino sand-silt mixtures interpreted using Eq. (10) are plotted in Fig. 11a (dashed curves) corresponding to the following values of β: β = 1.72 and β = 0.68, respectively. Superimposed in the same figure are the curves suggested by Seed et al. [76] (solid curves) corresponding to β values equal to 0.6 and 1, respectively. It can be noticed that a lot of experimental data is located above the upper bound curve recommended for clean sands, consistent with the findings previously reported by other authors [43,87].

To verify the applicability of stress-based models originally developed for clean sands to silty sands tested under initial applied static shear stresses, plots of residual pore water pressure ratio, $R_{u,res}$, versus cycle ratio, N/N_f, were given in Fig. 11b to 11d for Ticino sand-silt mixtures with different magnitudes of the initial static shear stress (α=0.10–0.30).

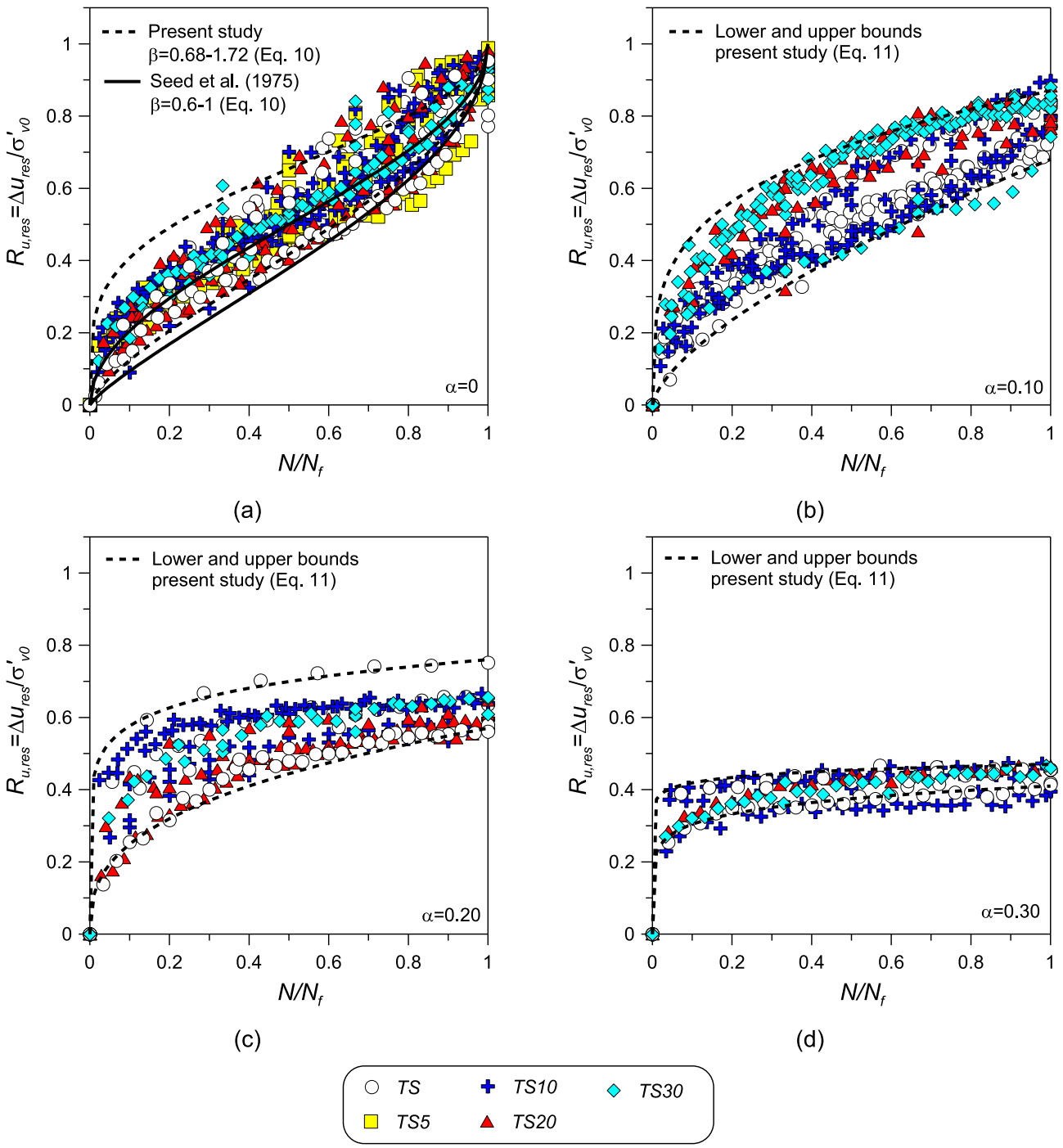

Fig. 11. Residual cyclic excess pore water pressure ratio versus normalized number of cycles under several α levels for Ticino-fines mixtures.

A careful analysis of the test data reported in Fig. 11b to 11d highlights some interesting features of the excess pore pressure development of the silty sand specimens subjected to initial static shear stress ($\alpha \neq 0$). In particular, the corresponding curves do not exhibit the typical biconcave trend shape in the normalized plots, but the residual pore pressure ratio increases rapidly during the early stage of the tests and, subsequently, it approaches more gradually the limiting $R_{u,lim}$ value.

Thus, to predict more reliably and satisfactorily the $R_{u,res}$ in non-plastic silty sands under an initial applied static shear stress, a new model was proposed in this study as follows:

$$R_{u,res} = c \bullet \left(\frac{N}{N_f}\right)^d \tag{11}$$

where c and d are two empirical parameters to be determined by back analysis of undrained cyclic test results.

The range of the parameters c and d corresponding to the lower and upper curves depicted in Fig. 11b–d are summarised in Table 2.

Table 2
Empirical parameters of the new proposed cyclic excess pore pressure generation model (Eq. (11) and Fig. 11) for silty sands.

$\alpha = \tau_{stat}/\sigma'_{v0}$	$c_{lower/upper}$	$d_{lower/upper}$
0.1	0.68-0.87	0.27-0.66
0.2	0.57-0.66	0.12-0.36
0.3	0.41-0.47	0.05-0.13

A further goal of the research was to define useful correlations between the empirical parameters c and d appearing in Eq. (11) and the key factors (i.e., e_0, f_c, α, CSR) affecting the development of the cyclic excess pore water pressures. Thus, a multivariable regression analysis was carried out to correlate the parameters c and d to all other factors. The relationships obtained for c and d are the following:

$$c = 1.433 - 0.686 \bullet e_0 - 1.955 \bullet \alpha + 0.00027 \bullet f_c^2 - 0.0099 \bullet f_c + 0.498 \bullet CSR \tag{12}$$

$$d = -0.301 + 1.172 \bullet e_0 - 1.644 \bullet \alpha - 0.00039 \bullet f_c^2 + 0.0162 \bullet f_c + 0.298 \bullet CSR$$

with a coefficient of determination R^2 equal to 0.94 and 0.71, respectively. More data is still needed to enhance the reliability of these relationships.

Fig. 12 shows $R_{u,lim}$, i.e. the residual excess *PWP* ratio detected in correspondence with the assumed liquefaction criterion, plotted against α. For α varying in the range 0-0.30, $R_{u,lim}$ decreased with the increase of α. The maximum value ($R_{u,lim} \approx 1$) was obtained only for $\alpha = 0$. This trend has been consistently observed for clean sands by other researchers (Vaid and Chern [9]; Pan and Yang [6], among others). A possible explanation can be found in the fact that the horizontal distance between the initial stress state and the critical state line of the tested specimens becomes increasingly shorter with the increase of α.

In order to interpret the experimental R_u data measured on non-plastic silty soils under an applied initial static shear stress by using *PWP* strain-based models, the approach proposed by Dobry [78] was adopted in the present study. In particular, Dobry [78] recommended an upper and lower boundary curve in the R_u versus γ domain based on the results of strain-controlled cyclic triaxial tests (solid lines in Fig. 13). In this figure, the symbol γ_{max} refers to the highest value of shear strain reached in a given cycle (in this case, $N = 10$) while $R_{u,res}$ is the residual *PWP* ratio evaluated at the same stage of the given cycle.

The residual excess *PWP* ratios of the sand-silt mixtures investigated in the present research for various global void ratios and fines content ($f_c \leq 30\%$) but without consideration of an applied initial static shear stress, are compared with the boundary curves proposed by Dobry [78] for clean sands (Fig. 13a). As can be seen, experimental data points lie in a relatively narrow band on the right-hand side of the suggested lower boundary curve for clean sand. These findings are consistent with those reported by other researchers from undrained cyclic triaxial [22,88] and simple shear tests [19] carried out on silty sands. Fig. 13a also shows that even experimental data of clean Ticino sand fall below the lower bound proposed by Dobry's model. This can be explained by considering the different strain paths followed by strain-controlled vs stress-controlled tests.

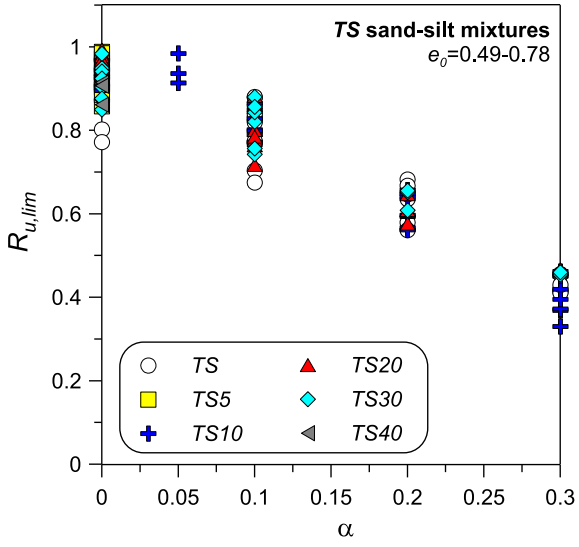

Fig. 12. Relationship between limiting residual pore water pressure ratio $R_{u,lim}$ and initial static shear stress ratio α for Ticino-fines mixtures (σ'_{v0}=100 kPa).

When the boundary curves proposed by Dobry [78] were compared with experimental data of the sand-silt mixtures with a consideration of an applied initial static shear stress (Fig. 13b–d), once again, the experimental data fell on the right-hand side of the Dobry's lower boundary curve with the distance from this latter increasing with the increase of α. It is interesting to note that a practically single best-fit trend line can be drawn to fit the experimental data for a given α value, irrespective of the f_c and e_0 values of the mixtures. The best-fit curves of the experimental data for each α value are represented as red dashed curves in Fig. 13 using the relationship proposed by Vucetic and Dobry [79]:

$$R_{u,res} = \frac{p \bullet f \bullet N \bullet F \bullet (\gamma - \gamma_{tvp})^s}{1 + f \bullet N \bullet F \bullet (\gamma - \gamma_{tvp})^s} \tag{13}$$

where γ is the cyclic shear strain, N is the number of loading cycles, and f is set to 1 or 2 for 1-D and 2-D cyclic loadings, respectively. The parameters p, F, and s are curve-fitting parameters. The volumetric threshold shear strain (γ_{tvp}) is defined as the shear strain below which no residual pore pressure is generated. Since the suggested range of values for γ_{tvp} is 0.01–0.02% for most soils [89], a value of γ_{tvp} equal to 0.01% was considered in the present study. The fitting parameters p, f, and F were given in Table 3 for each α value, regardless of initial void ratio and fines content ($\sigma'_{v0} = 100$ kPa).

5. Conclusions

A laboratory experimental research program was undertaken to improve the current knowledge on the combined effects of fines content and an applied initial static shear stress on the cyclic undrained response of non-plastic silty sands. Ticino sand (*TS*) with different percentages of non-plastic fines (up to 40%) was used as a test material for this study. The specimens were reconstituted by moist-tamping at different values of global void ratio ($e_0 = 0.49$–0.78) and subjected to different values of initial static shear stress (α = 0–0.30) under a single value of initial effective vertical stress ($\sigma'_{v0} = 100$ kPa).

The main results and conclusions drawn from this study are summarised below:

- Depending on the combination of initial void ratio, fines content, and degree of stress reversal in undrained cyclic loading, four typical failure patterns, namely flow liquefaction, limited flow liquefaction, cyclic mobility, and plastic strain accumulation, are observed. The most critical mechanisms are flow and limited flow liquefaction, which are characterised by an abrupt deformation without any warning signal. Cyclic flow liquefaction is observed in materials tested at higher void ratio ($e_0 \geq 0.68$) with fines content ranging from 20% to 30%. On the other hand, the cyclic mobility failure pattern is characterised by transient excursions of the stress path around the origin and significant cyclic shear strains. This type of failure pattern occurs in the case of specimens exhibiting a hardening behavior under stress reversal conditions. Finally, plastic strain accumulation is characterised by a large development of residual shear strains on the side of the applied initial static shear stress. This mechanism is generally observed when no shear stress-reversal condition ($\tau_{cyc} \leq \tau_{stat}$) or a limited shear stress reversal condition occurs.
- The cyclic resistance of silty sand (α=0) decreases with increasing initial void ratio and non-plastic silt up to the threshold fines content, f_{thre} ($\cong$24.5%), after which the trend reverses. The presence of an initial static shear stress can modify the effects of void ratio and fines

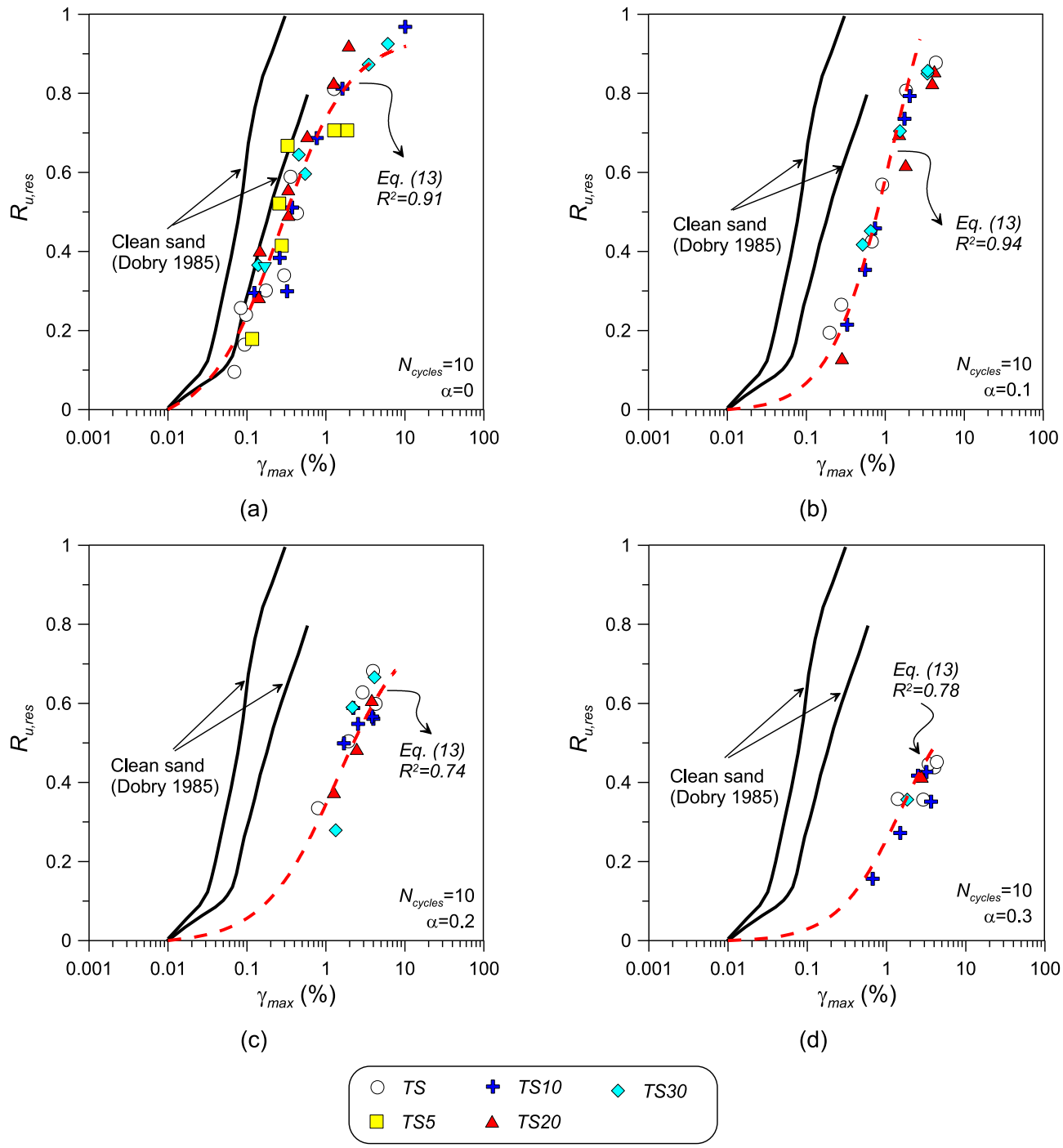

Fig. 13. Trend of residual pore water pressure ratios with maximum shear strains obtained in the present study compared with the upper and lower bound curves proposed by Dobry (1985) for clean sands: (a) α=0, (b) α=0.1, (c) α=0.2 and (d) α=0.3.

Table 3
Empirical parameters of the cyclic strain-based excess pore pressure generation model (Eq. (13) and Fig. 13) for silty sands.

α	p	f	F	s	γ_{tvp} (%)	R^2
0	0.945	1	0.3582	0.984	0.01	0.91
0.1	1.301	1	0.0825	1.128	0.01	0.94
0.2	0.818	1	0.0735	0.952	0.01	0.74
0.3	0.657	1	0.0646	1.094	0.01	0.78

content on cyclic resistance beneficially or detrimentally. In particular, it was found that *CRR* tends to decrease more significantly with a certain increment of void ratio for higher α values (i.e., α=0.2) than for lower ones (i.e., α=0). K_{fc} is the correction factor of *CRR* due to the change of f_c. The reduction of K_{fc} with $f_c < f_{thre}$ is more pronounced with increasing applied static stress ratio α.

- A parabolic correlation is proposed to capture satisfactorily (R^2>0.96) the trend of the K_{fc} - f_c relationships exhibited by Ticino sand-silt mixtures for different α values and fines contents (f_c = 0–40%; α = 0−0.30; σ'_{v0} = 100 kPa), regardless of initial void ratio of mixtures.

- An initial static shear stress correction factor, K_α, is introduced to characterise the effect of α on cyclic resistance of *TS*-fines mixtures, similar to clean sands [4]. In particular, K_α results in less than unity for all sand-silt mixtures (i.e., detrimental effect), whereas the effect of α is positive (i.e., beneficial) only when the void ratio and fines content are relatively low (e_0 = 0.55–0.60 for *TS* and *TS10*).
- A new correlation between *MSF* and M_w, using the M_w-N_f relationships proposed by Idriss [65], is introduced in the present study for non-plastic silty sands, regardless of initial void ratio, fines content, and initial static shear stress.
- The relationships between the residual pore pressure ratio $R_{u,res}$ and the normalized number of loading cycles N/N_f of non-plastic silty sands in the presence of an initial static shear stress ($\alpha \neq 0$) follows a different trend if compared with that observed for companion tests with α=0, reaching a limiting value ($R_{u,lim}$) which decreases when α increases. Thus, a new stress-based *PWP* generation model is herein proposed for quantifying the cyclic *PWP* development of silty sands under various static shear stress conditions in a satisfactory way.
- The relationships between the residual pore pressure ratio and the maximum shear strain evidence that the experimental results are not affected by e_0, *CSR*, and f_c but only by α. Thus, the values of model calibration parameters of the Vucetic and Dobry [79] *PWP* generation model are provided, taking into account the influence of the initial static shear stress ratio α.

The findings gathered in this study are based on specific materials (Ticino sand and *TS* with non-plastic fines), sample preparation method (moist tamping), testing apparatus (constant volume CSS), testing procedure conditions (stress-controlled cyclic loading), and initial states (e_0, σ'_{v0}, α) of tests used for the experimental investigation. Additional studies considering other sands, reconstitution methods, and initial vertical effective stresses are required to confirm and/or better qualify these conclusions.

Author Statement

Giuseppe Tomasello: Methodology, Investigation, Data curation, Writing – original draft, Writing – review & editing. Daniela Dominica Porcino: Conceptualization, Methodology, Writing – original draft, Writing – review & editing, Supervision.

Declaration of competing interest

The authors declare that they have no known competing financial interests or personal relationships that could have appeared to influence the work reported in this paper

Data availability

Data will be made available on request.

References

[1] Kokusho T. Earthquake-induced flow liquefaction in fines-containing sands under initial shear stress by lab tests and its implication in case histories. Soil Dynam Earthq Eng 2020;130(2020):105984. https://doi.org/10.1016/j.soildyn.2019.105984.

[2] Porcino D, Diano V. Laboratory study on pore pressure generation and liquefaction of low-plasticity silty sandy soils during the 2012 earthquake in Italy. J Geotech Geoenviron Eng 2016;142(10):04016048. https://doi.org/10.1061/(ASCE)GT.1943-5606.0001518.

[3] Chiaro G, Koseki J. Prediction of earthquake-induced liquefaction for level and gently sloped ground. In: Chin CY, editor. 19th New Zealand geotechnical society symposium. New Zealand: Institution of Professional Engineers New Zealand; 2013. p. 61–8.

[4] Seed HB. Earthquake-resistant design of earth dams. In: International conferences on recent advances in geotechnical earthquake engineering and soil dynamics. Missouri: University of Missouri; 1981.

[5] Castro G. Liquefaction and cyclic mobility of saturated sands. J Geotech Geoenviron Eng 1975;101(GT6):551–69.

[6] Pan K, Yang ZX. Effects of initial static shear on cyclic resistance and pore pressure generation of saturated sand. Acta Geotechnica 2018;13:476–87. https://doi.org/10.1007/s11440-017-0614-5.

[7] Wei X, Yang J. Cyclic behavior and liquefaction resistance of silty sands with presence of initial static shear stress. Soil Dynam Earthq Eng 2019;122:274–89. https://doi.org/10.1016/j.soildyn.2018.11.029. 2019.

[8] Yang ZX, Pan K. Flow deformation and cyclic resistance of saturated loose sand considering initial static shear effect. Soil Dynam Earthq Eng 2017;92:68–78. https://doi.org/10.1016/j.soildyn.2016.09.002. 2017.

[9] Vaid YP, Chern JC. Effect of static shear on resistance to liquefaction. Soils Found 1983;23(1):47–60. https://doi.org/10.3208/sandf1972.23.47.

[10] Hyodo YP, Tanimizu H, Yosufuku N, Murata H. Undrained cyclic and monotonic triaxial behaviour of saturated loose sand. Soils Found 1994;34(1):19–32.

[11] Vaid YP, Stedman JD, Sivathayalan S. Confining and static shear effects in cyclic liquefaction. Can Geotech J 2001;38(3):580–91. https://doi.org/10.1139/t00-120.

[12] Sivathayalan D, Ha D. Effect of static shear stress on the cyclic resistance of sands in simple shear loading. Can Geotech J 2011;48(10):1471–84. https://doi.org/10.1139/t11-056.

[13] Yang J, Sze HY. Cyclic behaviour and resistance of saturated sand under non-symmetrical loading conditions. Geotechnique 2011;61(1):59–73. https://doi.org/10.1680/geot.9.P.019.

[14] Umar M, Chiaro G, Kiyota T, Ullah N. Deformation and cyclic resistance of sand in large-strain undrained torsional shear tests with initial static shear stress. Soils Found 2021;61(3):765–81. https://doi.org/10.1016/j.sandf.2021.02.008.

[15] Nong Z-Z, Park S-S, Lee D-E. Comparison of sand liquefaction in cyclic triaxial and simple shear tests. Soils Found 2021;61(4):1071–85. https://doi.org/10.1016/j.sandf.2021.05.002.

[16] Yang J, Sze HY. Cyclic strength of sand under sustained shear stress. J Geotech Geoenviron Eng 2011;137(12):1275–85. https://doi.org/10.1061/(ASCE)GT.1943-5606.0000541.

[17] Papadopoulou A, Tika T. The effect of fines on critical state and liquefaction resistance characteristics of non-plastic silty sands. Soils Found 2008;48(5):713–25. https://doi.org/10.3208/sandf.48.713.

[18] Huang AB. The seventh james K. Mitchell lecture: characterization of silt/sand soils. In: Lehane Acosta-Martinez, Kelly, editors. Geotechnical and geophysical site characterization 5, sidney: 2016. Australian Geomechanics Society; 2016. p. 3–18.

[19] Porcino DD, Diano V. The influence of non-plastic fines on pore water pressure generation and undrained shear strength of sand-silt mixtures. Soil Dynam Earthq Eng 2017;101:311–21. https://doi.org/10.1016/j.soildyn.2017.07.015. 2017.

[20] Porcino DD, Triantafyllidis T, Wichtmann T, Tomasello G. Application of critical state approach to liquefaction resistance of sand-silt mixtures under cyclic simple shear loading. J Geotech Geoenviron Eng 2021;143(3):04020177. https://doi.org/10.1061/(ASCE)GT.1943-5606.0002470.

[21] Porcino DD, Triantafyllidis T, Wichtmann T, Tomasello G. Using different state parameters for characterizing undrained static and cyclic behavior of sand with non-plastic fines. Soil Dynam Earthq Eng 2022;159(2022):107318. https://doi.org/10.1016/j.soildyn.2022.107318.

[22] Dash HK, Sitharam TG. Undrained cyclic pore pressure response of sand-silt mixtures: effect of nonplastic fines and other parameters. Geotech Geol Eng 2009;27(4):501–17. https://doi.org/10.1007/s10706-009-9252-5.

[23] Xenaki VC, Athanasopoulos GA. Liquefaction resistance of sand–silt mixtures: an experimental investigation of the effect of fines. Soil Dynam Earthq Eng 2003;23(3):1–12. https://doi.org/10.1016/S0267-7261(02)00210-5.

[24] Carraro JAH, Bandini P, Salgado R. Liquefaction resistance of clean and nonplastic silty sands based on cone penetration resistance. J Geotech Geoenviron Eng 2003;129(11):965–76. https://doi.org/10.1061/(ASCE)1090-0241. 2003)129:11(965.

[25] Chien L-K, Oh Y-N, Chang C-H. Effects of fines content on liquefaction strength and dynamic settlement of reclaimed soil. Can Geotech J 2002;39(1):254–65. https://doi.org/10.1139/t01-083.

[26] Thevanayagam S, Shenthan T, Mohan S, Liang J. Undrained fragility of clean sands, silty sands, and sandy silts. J Geotech Geoenviron Eng 2002;128(10):849–59. https://doi.org/10.1061/(ASCE)1090-0241. 2002)128:10(849.

[27] Wei X, Yang J. Characterizing the effects of fines on the liquefaction resistance of silty sands. Soils Found 2019;59(6):1800–12. https://doi.org/10.1016/j.sandf.2019.08.010.

[28] Yang J, Wei LM, Dai BB. State variables for silty sands: global void ratio or skeleton void ratio? Soils Found 2015;55(1):99–111. https://doi.org/10.1016/j.sandf.2014.12.008.

[29] Hazirbaba K. Pore pressure generation characteristics of sands and silty sands: a strain approach. PhD Thesis. The University of Texas at Austin; 2005.

[30] Polito CP. The effects of non-plastic and plastic fines on the liquefaction of sandy soils. PhD Thesis. Virginia Institute and State University; 1999.

[31] Yang S, Lacasse S, Sandven R. Determination of the transitional fines content of mixtures of sand and non-plastic fines. Geotech Test J 2006;29(2):102–7.

[32] Mohammadi A, Qadimi A. A simple critical state approach to predicting the cyclic and monotonic response of sands with different fines contents using the equivalent intergranular void ratio. Acta Geotechnica 2015;10:587–606. https://doi.org/10.1007/s11440-014-0318-z.

[33] Zuo L, Baudet BA. Determination of the transitional fines content of sand-non plastic fines mixtures. Soils Found 2015;55(1):213–9. https://doi.org/10.1016/j.sandf.2014.12.017.

[34] Porcino DD, Tomasello G, Wichtmann T. An insight into the prediction of limiting fines content for mixtures of sand with non-plastic fines based on monotonic and cyclic tests. In: Moraci N, Silvestri F, editors. Earthquake geotechnical engineering for protection and development of environmant and constructions. Rome: 2019 Associazione Geotecnica Italiana; 2019. p. 4540–7.

[35] Porcino DD, Diano V, Tomasello G. Effect of non-plastic fines on cyclic shear strength of sand under an initial static shear stress. In: Wu W, Yu H-S, editors. Proceeding of China-europe conference on geotechnical engineering, springer series in geomechanics and geoengineering. Cham: Springer; 2018. p. 597–601.
[36] Pan K, Zhou GY, Yang ZX, Cai YQ. Comparison od cyclic liquefaction behavior of clean and silty sands considering static shear effect. Soil Dynam Earthq Eng 2020; 139(2020):106338. https://doi.org/10.1016/j.soildyn.2020.106338.
[37] Pan XD, Chen JQ, Pan K, Xu X, Jiang JW, Yang ZX. Cyclic flow behavior of anisotropically consolidated sand with small amount of fines. Soil Dynam Earthq Eng 2021;143(2021):106778. https://doi.org/10.1016/j.soildyn.2021.106778.
[38] Sze HY, Yang J. Failure modes of sand in undrained cyclic loading: impact of sample preparation. J Geotech Geoenviron Eng 2014;140(1):152–69. https://doi.org/10.1061/(ASCE)GT.1943-5606.0000971.
[39] Vaid YP, Finn WDL. Static shear and liquefaction potential. J Geotech Eng Div 1979;105(10):1233–46. https://doi.org/10.1061/AJGEB6.0000868.
[40] Park S-S, Nong Z-Z, Lee D-E. Effect of vertical effective and initial static shear stresses on the liquefaction resistance of sands in cyclic direct simple shear tests. Soils Found 2020;60(6):1588–607. https://doi.org/10.1016/j.sandf.2020.09.007.
[41] Yang ZX, Pan K. Energy-based approach to quantify cyclic resistance and pore pressure generation in anisotropically consolidated sand. Jounal of Materials in Civil Engineering 2018;30(9):04018203. https://doi.org/10.1061/(ASCE)MT.1943-5533.0002419.
[42] Sassa K, Wang G, Fukuoka H, Vankov DA. Shear-displacement-amplitude dependent pore-pressure generation in undrained cyclic loading ring shear tests: an energy approach. J Geotech Geoenviron Eng 2005;131(6):750–61. https://doi.org/10.1061/(ASCE)1090-0241. 2005)131:6(750.
[43] Polito CP, Green RA, Lee JL. Pore pressure generation models for sands and silty soils subjected to cyclic loading. J Geotech Geoenviron Eng 2008;134(10): 1490–500. https://doi.org/10.1061/(ASCE)1090-0241. 2008)134:10(1490.
[44] Porcino DD, Tomasello G, Diano V. Key factors affecting prediction of seismic pore water pressures in silty sands based on damage parameters. Bull Earthq Eng 2018; 16:5801–19. https://doi.org/10.1007/s10518-018-0411-z.
[45] Porcino DD, Tomasello G, Farzalizadeh R. Pore-pressure generation od sands subjected to cyclic simple shear loading: an energy approach. In: Wang L, Zhang JM, Wang R, editors. Proceedings of the 4th international conference on performance based design in earthquake geotechnical engineering. Beijing: Springer Cham; 2022. p. 1674–82.
[46] Zhang J, Cao J, Huang S. Effects of initial shear stress and vibration frequency on the dynamic pore-water pressure of saturated sands. Adv Civ Eng 2018;2018: 6124809. https://doi.org/10.1155/2018/6124809.
[47] Tomasello G. Critical state approach and equivalent granular state theory for predicting the undrained cyclic and monotonic behaviour of non-plastic silty sands. PhD Thesis. University of Messina; 2021.
[48] Haeri SM, Ghafouri SMHS, Nikoonejad K. Effect of initial static shear stress on undrained cyclic resistance of well graded, medium dense gravelly soils. Tehran: 11th Internation Congress on Civil Engineering; 2018.
[49] ASTM D4253. Standard test methods for maximum index density and unit weight of soils using vibratory table. West Conshohocken, PA, USA: ASTM International; 2006.
[50] ASTM D4254. Standard test methods for minimum index density and unit weight of soils and calculations of relative density. West Conshohocken, PA, USA: ASTM International; 2000.
[51] McGeary RK. Mechanical packing of spherical particles. J Am Ceram Soc 1961;44: 513–22. https://doi.org/10.1111/j.1151-2916.1961.tb13716.x.
[52] Ni Q, Tan TS, Dasari GR, Hight DW. Contribution of fines to the compressive strength of mixed soils. Geotechnique 2004;54(9):561–9. https://doi.org/10.1680/geot.2004.54.9.561.
[53] Porcino D, Caridi G, Malara M, Morabito E. An automated control system for undrained monotonic and cyclic simple shear tests. In: DeGroot DJ, DeJong JT, Frost JD, Baise LG, editors. Geotechnical engineering in the information technology age. Reston: American Society of Civil Engineering; 2006. p. 185–90.
[54] Finn WDL. Aspects of constant volume cyclic simple shear. In: Khosla V, editor. Advances in the art of testing soils under cyclic conditions. Cleaveland: Herron Consultans; 1985. p. 74–98.
[55] Dyvik R, Berre T, Lacasse S, Raadim B. Comparison of truly undrained and constant volume direct simple shear tests. Geotechnique 1987;37:3–10. https://doi.org/10.1680/geot.1987.37.1.3.
[56] Moussa AA. Equivalent drained-undrained shearing resistance of sand to cyclic simple shear loading. Geotechnique 1975;25(3):485–94. https://doi.org/10.1680/geot.1975.25.3.485.
[57] Finn WD, Vaid YP. Liquefaction potential from drained constant volume cyclic simple shear tests. New Delhi, Jan: Proc., 6th World Conference on Earthquake Engineering; 1977. p. 7–12.
[58] Finn WD, Vaid YP, Bhatia S. Constant volume cyclic simple shear testing. San Francisco, California: Proc., 2nd Int. Conference on Microzonation; 26 . p. 839–51.
[59] Ladd RS. Preparing test specimens using undercompaction. Geotech Test J 1978;1 (1):16–23. https://doi.org/10.1520/GTJ10364J.
[60] Diano V. Influence of non-plastic fines on monotonic and cyclic behaviour of silty sands. PhD Thesis. Mediterranean University of Reggio Calabria; 2017.
[61] Porcino DD, Diano V, Triantafyllidis T, Wichtmann T. Predicting undrained static response of sand with non-plastic fines in terms of equivalent granular state. Acta Geotechnica 2020;15:867–82. https://doi.org/10.1007/s11440-019-00770-5.
[62] NCR (National Research Council). Liquefaction of soils during earthquakes. Washington: National Academy Press; 1985.
[63] Towhata I, Gunji K, Hernandez YA, Yamada S. Laboratory tests on cyclic undrained behavior of looses and with cohesionless silt and its application to assessment of seismic performance of subsoil. In: Proceedings of the New Zealand - Japan workshop on soil liquefaction during recent large - scale earthquakes. NZ: University of Auckland; Dec. 2–3, 2013.
[64] Seed HB, Idriss IM. Ground motions and soil liquefaction during earthquakes. Oakland, California: Earthquake Engineering Research Institute; 1982.
[65] Idriss IM. An update to the seed-idriss simplified procedure for evaluating liquefaction potential. In: Proceedings of TRB workshop on new approaches to liquefaction. Washington DC: Federal Highway Administration; 1999.
[66] Idriss IM, Boulanger RW. Soil liquefaction during earthquakes. Earthquake Engineering Research Institute; 2008.
[67] Youd TL, et al. Liquefaction resistance of soils: summary report from the 1996 NCEER and 1998 NCEER/NSF workshops on evaluation of liquefaction resistance of soils. J Geotech Geoenviron Eng 2001;127:817–33. https://doi.org/10.1061/(ASCE)1090-0241(2001)127:10(817).
[68] Idriss IM, Boulanger RW. Semi-empirical procedures for evaluating liquefaction potential during earthquakes. Soil Dynam Earthq Eng 2006;26(2–4):115–30. https://doi.org/10.1016/j.soildyn.2004.11.023.
[69] Bouckovalas GD, Andrianopoulos KI, Papadimitriou AG. A critical state interpretation for the cyclic liquefaction resistance of silty sands. Soil Dynam Earthq Eng 2003;23(2):115–25. https://doi.org/10.1016/S0267-7261(02)00156-2.
[70] Polito CP, Martin JR. A reconciliation of the effects of non-plastic fines on the liquefaction resistance of sands reported in the literature. Earthq Spectra 2003;19 (3):635–51. https://doi.org/10.1193/1.1597878.
[71] Wei X, Yang J, Zhou Y-G, Chen Y. Influence of particle-size disparity on cyclic liquefaction resistance of silty sands. Géotech Lett 2020;10(2):155–61. https://doi.org/10.1680/jgele.19.00076.
[72] Rahman MM, Lo SR. The prediction of equivalent granular steady state line of loose sand with fines. Geomechanics Geoengin 2008;3(3):179–90. https://doi.org/10.1080/17486020802206867.
[73] Harder Jr LF, Boulanger RW. Application of K_σ and K_α correction factors. In: Youd TL, Idriss IM, editors. Proceedings of the NCEER workshop on evaluation of liquefaction resistance of soils. Buffalo, N.Y.: National Center for Earthquake Engineering Research, State University of New York at Buffalo; 1997. p. 167–90.
[74] Tomasello G, Porcino DD. Influence of sloping ground conditions on cyclic behavior of sand under simple shear loading. Soil Dynam Earthq Eng 2022;163 (2022):107516. https://doi.org/10.1016/j.soildyn.2022.107516.
[75] Porcino D, Caridi G, Ghionna VN. Undrained monotonic and cyclic simple shear behavior of carbonate sand. Geotechnique 2008;58:635–44. https://doi.org/10.1680/geot.2007.00036.
[76] Seed HB, Martin PP, Lysmer J. In: The generation and dissipation of pore-water pressures during soil liquefaction. Univ. of California. 75–26. Berkeley, CA: Geotechnical Report No. EERC; 1975.
[77] Baziar MH, Shahnazari H, Sharafi H. A laboratory study on the pore pressure generation model for Firouzkooh silty sands using hollow torsional test. Int J Civ Eng 2011;9(2):126–34.
[78] Dobry R. Liquefaction of soils during earthquakes. Rep. No. CETS-EE-001. Washington, DC: National Research Council (NRC), Committee on Earthquake Engineering; 1985.
[79] Vucetic M, Dobry R. Pore pressure build-up and liquefaction at level sandy sites during earthquakes. Troy, NY: Dept. of Civil Engineering, Rensselaer Polytechnic Institute; 1986. Research report CE-86-3.
[80] Berrill JB, Davis RO. Energy dissipation and seismic liquefaction of sands: revised model. Soils Found 1985;25(2):106–18.
[81] Green RA, Mitchell JK, Polito CP. An energy-based excess pore-water pressure generation model for cohesionless soils. In: Smith DW, Carter JP, editors. Proc., John booker memorial symp.-developments in Theoretical geomechanics. Rotterdam, Netherlands: Balkema; 2000. p. 383–90.
[82] Elgamal A, Yang Z, Parra E, Ragheb A. Modeling of cyclic mobility in saturated cohesionless soils. Int J Plast 2003;19(6):883–905. https://doi.org/10.1016/S0749-6419(02)00010-4.
[83] Boulanger RW, Ziotopoulou K. PM4Sand (version 3): a sand plasticity model for earthquake engineering applications. Center for Geotechnical Modeling: University of California at Davis; 2015. Report No. UCD/CGM-15/01.
[84] Ishihara K. Liquefaction on flow failure during earthquake. Geotechnique 1993;43 (3):351–415. https://doi.org/10.1680/geot.1993.43.3.351.
[85] Boulanger RW, Idriss IM. Liquefaction criteria for silts and clays. Journal of Geotechnical and Geoenvironmenatl Engineering 2006;132(11):1413–26. https://doi.org/10.1061/(ASCE)1090-0241. 2006)132:11(1413.
[86] Booker JR, Rahman MS, Seed HB. In: GADFLEA-a computer program for the analysis of pore pressure generation and dissipation during cyclic or earthquake loading. 76–24. Berkeley, CA: Univ. of California; 1976. EERC Report No.
[87] Park T, Park D, Ahn J-K. Pore pressure model based on accumulated stress. Bull Earthq Eng 2015;13:1913–26. https://doi.org/10.1007/s10518-014-9702-1.
[88] Cetin KO, Bilge HT. Cyclic large strain and induced pore pressure models for saturated clean sands. J Geotech Geoenviron Eng 2012;138(3):309–23. https://doi.org/10.1061/(ASCE)GT.1943-5606.0000631.
[89] Dobry R, Ladd RS, Yokel FY, Chung RM, Powell D. Prediction of pore-water pressure buildup and liquefaction of sands during earthquakes by the cyclic strain method. U.S. Dept. of Commerce, Washington, D.C. In: NBS building science series, 138. National Bureau of Standards; 1982.